EXFOLIATION AND MORPHOLOGICAL EVOLUTION FROM GRAPHITE TO GRAPHENE IN COMPACTED REACTORS

A Thesis

by

JOSHUA TYLER HOPE

Submitted to the Office of Graduate and Professional Studies of
Texas A&M University
In partial fulfillment of the requirements for the degree of

MASTER OF SCIENCE

Chair of Committee,	Micah Green
Committee Members,	Patrick Shamberger
	Zhengdong Cheng
Head of Department,	Ibrahim Karaman

May 2019

Major Subject: Materials Science and Engineering

ABSTRACT

Since its discovery in 2004, graphene has shown promise for technological advances in numerous fields such as advanced electronics, membranes, structural composites, and energy storage. Graphene's unique physical and chemical structure that allow for it to have an extraordinary combination of mechanical, electrical, and thermal properties. As the applications for graphene spread, a reliable method to produce large quantities of defect free, single layer graphene has trailed behind. Numerous top-down(mechanical cleavage and liquid phase exfoliation) and bottom-up(chemical vapor deposition) approaches have been used to produce graphene with various success rates. As with all materials, there are trade-offs between the quality and quantity of the graphene that is being produced with each method.

The goal of this research is to better understand scalable graphene production through electrochemical containment exfoliation. The produced graphene has shown large lateral size, low defects, and only a few layers thick. This production method has shown to be promising due to its potential scalability, low costs, and simplicity. Through the development of a new generation electrochemical reactor, we studied the electrical and diffusion limitations of various compacted graphite bed thicknesses. We also evaluated the rate of graphite expansion and the morphological changes to the graphite bed. The properties of the material produced through this unique method can be exploited and tailored for applications such as composites and supercapacitors.

ACKNOWLEDGEMENTS

Dr. Green, thank you for the advice and encouragement that you have given me. You have always challenged me to push my limits and find another way to look at a problem. You taught me how to see each problem in a different light and how to search for the true underlying issue. I have learned more than just scientific concepts from you. I have learned many valuable skills during my research with you and I am grateful for all that you have done.

I would also like to thank Dr. Wanmei Sun for all of our brainstorming sessions and advice on our projects. You have given me new insight into how to conduct my research and present my work in the best manner. I am thankful to Dr. Taruna Bansala for your valuable input on this research. I want to acknowledge all of my colleagues, current and past members of the Green group. Special thanks to Martin, Smit, Devon, and Shaan for all the help in the lab and advice when the experiments didn't cooperate. To the countless undergraduates who have worked in the Green group, thank you for all those joyful moments. I am thankful for Dr. Rohan Hule of ExxonMobil for helpful input on this project. I would also like to thank ExxonMobil for funding this project.

To my mom and dad, you are my original source of inspiration. You are the ones to fuel my thirst for knowledge and intellectual curiosity. You have pushed me through the years to achieve more than I thought was possible. To by brothers and sister, thanks for listening to all of my crazy ideas and encouraging me to persevere.

CONTRIBUTORS AND FUNDING SOURCES

Contributors

This work was supported by a thesis committee consisting of Professor Micah Green of the Department of Chemical Engineering, Professor Patrick Shamberger of the Department of Materials Science and Engineering, and Professor Zhengdong Cheng of the Department of Materials Science and Engineering.

The analyses depicted in Chapter 3 were conducted in part by Thomas Achee and Wanmei Sun of the Department of Chemical Engineering and were published in 2018 in Scientific Reports. The supercapacitor data analyzed for Chapter 4 was provided by Wanmei Sun. The experiments tested in Chapter 4 were completed with the aid of Shaan Kewalramani of the Department of Chemical Engineering.

All other work conducted for the thesis was completed by the student independently.

Funding Sources

This work was made possible in part by ExxonMobil.

TABLE OF CONTENTS

Page

LIST OF FIGURES

Page

LIST OF TABLES

Page

CHAPTER I

INTRODUCTION

Graphene is the first two-dimensional atomic crystal and was isolated in 2004 by Andre Geim and Konstantin Novoselov.[1, 2] This one-atom thin sheet of sp^2 hybridized carbon produces a honeycomb structure with outstanding theoretical mechanical, electrical, thermal, and optical properties.[3, 4] Since the discovery in 2004, these extraordinary properties have been experimentally verified from graphene produced from exfoliated highly oriented pyrolytic graphite (HOPG) or by chemical vapor deposition.[5, 6] Graphene has been hyped as a solution to technological advances that have previously been limited by the available materials. The mechanical, electrical, thermal, and optical properties of graphene are unlike any researched material. This could lead to applications in energy storage, structural composites, and advanced electronics.[7-13]

The pristine graphene production method must be chosen based on the target application, which is also scalable for industry. For example, mechanical exfoliation can produce monolayer graphene sheets with few additional defects that could be useful for electronics.[4, 14, 15] One reason that producing graphene is so lucrative is that the reactants are very cheap. In the top-down processing methods, battery grade flake graphite can be bought at $5,000-$20,000 per tonne.[7, 16] The prospect of producing graphene from graphite has sparked the interest of graphite mining companies all over the world.

We provide insight to how the development of a second-generation reactor that utilizes electrochemical containment exfoliation is scalable in the production of high quality few-layer graphene. The effects of compaction, electrical contact, electrolyte diffusion, and graphite-to-graphene expansion rates are evaluated. We verify the quality of the produced sheets through traditional characterization methods and apply the material to supercapacitor technology.

CHAPTER II

GRAPHENE STRUCTURE, PROPERTIES, CHARACTERIZATION, AND APPLICATIONS

2.1 History of Graphene

What began as an unconventional idea in a lab at the University of Manchester has challenged what scientists' thought was possible for nano-scale materials.[17, 18] The scientific community believed that it was impossible for such thin 2D crystalline material to be thermodynamically favorable, and thus could not exist.[19] It was believed that an atomic thin 2D crystal would not be able to sustain the thermal fluctuations at room temperature and its structure would collapse due to atomic dislocations and defects.[20, 21] In 2004, Andre Geim and Konstanin Novoselov attempted to make thinner flakes of graphite with the aid of sticky Scotch tape in order to investigate its electrical properties.[1, 2, 11, 17, 22] This "scotch-tape" method used mechanical cleavage to produce pristine graphene from highly oriented pyrolytic graphite (HOPG).[2, 11] This fascinating idea led to these scientists to win a joint Nobel prize in Physics in 2010 for their ground-breaking experiments.[23] The subsequent work revealed a material that possessed extraordinary mechanical, electrical, thermal, and optical properties. Since then, there has been a tremendous effort to design a scalable process for high-quality graphene production.

2.2 Structure of Graphene

2.2.1 Atomic Structure

Each carbon is bonded to three additional carbon atoms through covalent σ bonds with a distance of 0.142 nm.[24, 25] Additionally, each carbon shares a double bond with adjacent carbons through its π orbital. These double bonds create a delocalized network of π electrons.[24] In pristine graphene, the carbon atoms on the basal plane of a graphene sheet are all sp^2 hybridized and the carbon atoms located on the edges of the graphene sheet are sp^3 hybridized. While graphene may be described as a 2D plane, studies have shown that freestanding graphene sheets exhibit rippling effects (**Figure 1**).[26]

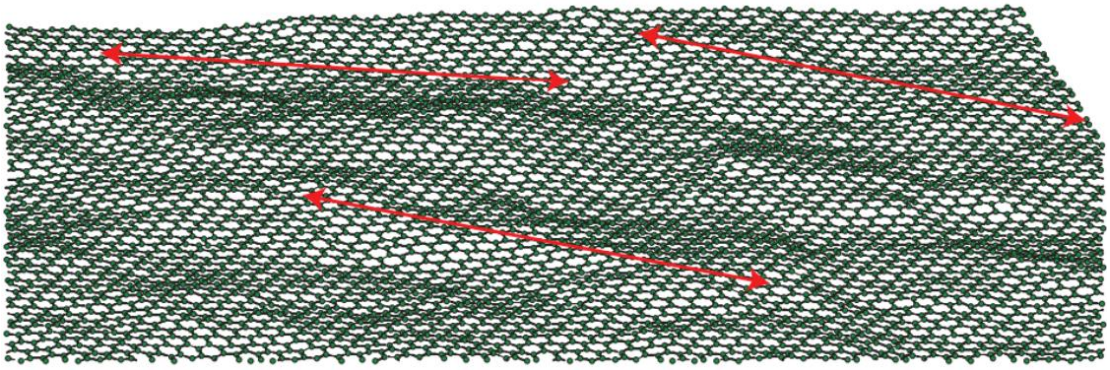

Figure 1: Rippling effects on a sheet of graphene (reproduced with permission from Fasolino *et al*.[26])

Graphene can be seen as the basic building block for carbon allotropes such as fullerenes, carbon nanotubes, and graphite. Whereas fullerenes and carbon nanotubes are easily differentiated from graphene, graphite needs to be clearly defined. Graphite is many layers of graphene stacked on top of each other with an interlayer spacing of 0.335 nm.[19, 24, 27] However, the stacking will affect the material properties which will be discussed in the following sections. Because the material properties change with the

number of stacked layers, the nomenclature of graphene also changes with the number of layers. Recently, the International Organization for Standardization (ISO) launched the first standard for 2D materials nomenclature with the following classification: [28]

- Graphene: single layer of carbon atoms with each atom bound to three neighbors in a honeycomb structure
- Bilayer Graphene: two well-defined stacked graphene layers
- Few-layer graphene: consisting of three to ten well-defined stacked graphene layers, approximately between 1 nm to 3 nm thick
- Graphene Nanoplatelet: typically have a thickness between 3 nm to 10 nm and lateral dimensions ranging from ≈ 100 nm to 100 μm

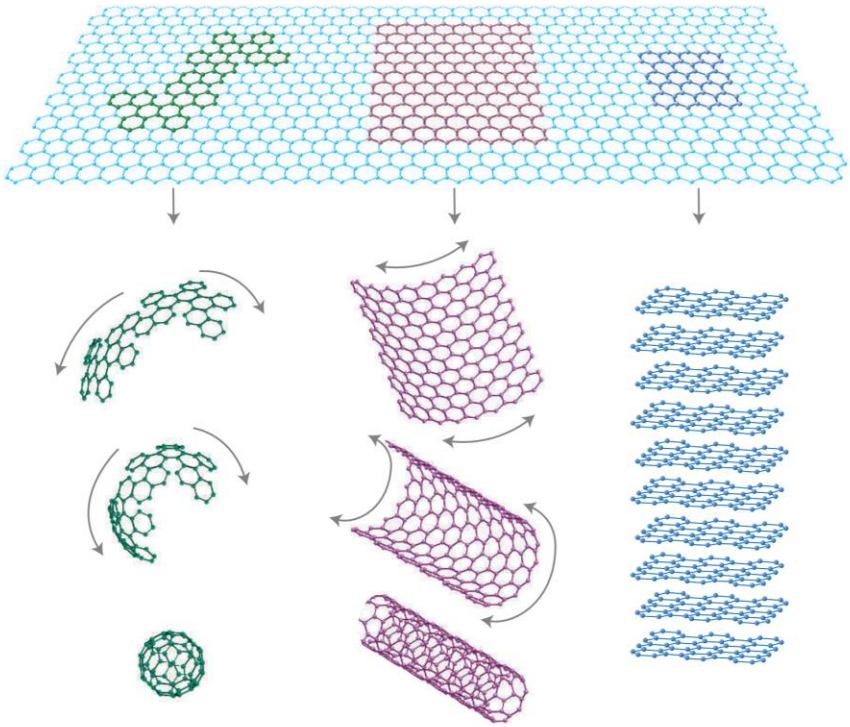

Figure 2: Graphene as the building block carbon allotropes. Graphene can be wrapped to form 0D Buckyballs, rolled into 1D CNTs, or stacked into 3D graphite. (reproduced with permission from Geim *et al*.[2])

2.2.2 Electronic Structure

A layer of graphene acts as an intrinsic semiconductor in that it has one type of electron and one type of hole as charge carriers. One of the most interesting aspects of the graphene problem is that its low-energy excitations are massless, chiral, Dirac fermions.[24, 27] The low defect density of graphene allows for exceptionally high carrier mobilities. Carrier mobilities up to 15,000 cm^2/Vs have been measured at ambient conditions.[24-27] Graphene can display exceptionally high carrier mobility due to a phenomenon known as ballistic transport, in which carriers can travel long interatomic distances without being scattered.[29] There are a myriad sources of disorder in graphene

and can vary from ordinary effects commonly found in semiconductors, such as ionized impurities in the substrate, to adatoms and various molecules adsorbed in the graphene surface, to more unusual defects such as ripples associated with the soft structure of graphene.[27] Thus the quality of graphene and the interactions with the surroundings will impact the carrier mobility. A mechanically-exfoliated freestanding graphene layer was subjected to vacuum in order to minimize impurity-induced scattering and carrier mobilities as high as 200,000 cm^2/Vs were obtained.[19, 25]

Graphene is also a zero-energy semiconductor. The conduction and valence bands of graphene are symmetrical and meet at the Dirac point (neutrality point). The graphene structure is ambipolar, meaning that the charge carrier can be tuned between electrons and holes depending on the applied gate voltage. A negative gate bias causes the holes to be the dominant carriers and a positive gate bias causes electrons to act as carriers.[19, 24, 29]

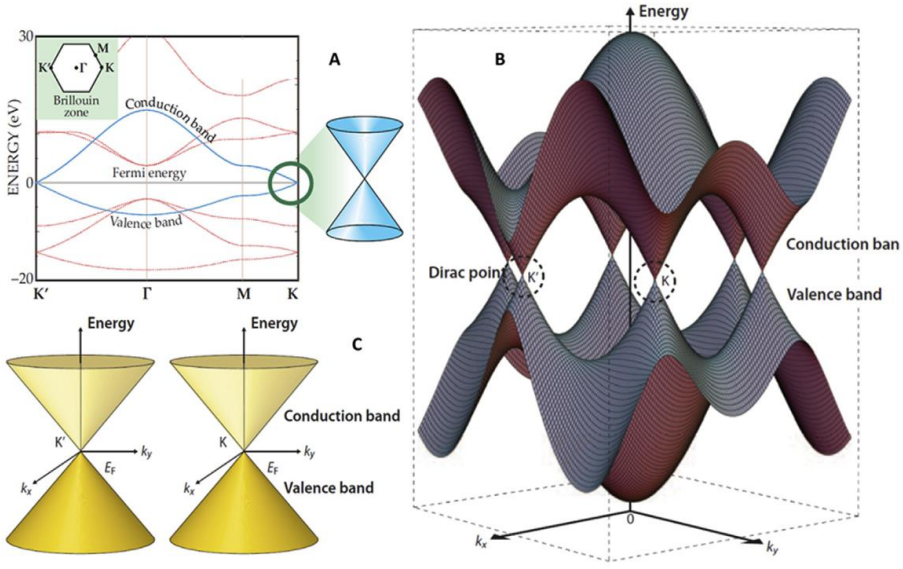

Figure 3: Band structure of graphene near the Fermi level. (a)2D schematic, (b) 3D schematic, and (c) Dirac cone of K and K', which correspond to the Fermi level. (reproduced with permission from Wang *et al*.[29])

2.2.3 Chemical Structure

Pristine graphene has a very low chemical reactivity due to its π bond network. Additionally, the lack of curvature in graphene morphology inhibits its reactivity in comparison to carbon structures like CNTs and fullerenes.[19, 24, 25] As expected, graphene is hydrophobic and prone to agglomeration in water. However, like all materials, graphene is prone to defects that can increase its reactivity. Graphene has been shown to contain vacancies, adatoms, topological defects (pentagons and heptagons instead of the usual hexagonal ring), and impurities bonded to the structure (**Figure 4**).

As mentioned before, the carbon atoms on the basal plane and edges exhibit different bond hybridization. Carbon atoms at the edge are sp^3 hybridized are open to covalent functionalization and are thus more reactive.[4, 10, 30] It is less likely that the carbon atoms on the basal plane become functionalized since the transformation is energy consuming and disturbs the conjugated π system. In order for carbon atoms on the basal plane to become covalently functionalized, highly energetic species are needed to attack the π network of the basal plane.[10]

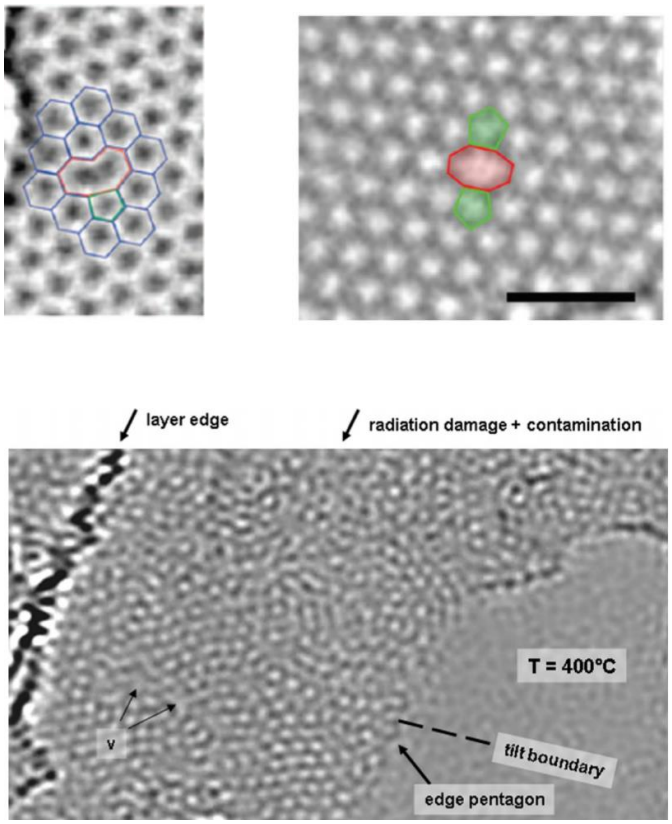

Figure 4: TEM images of defects in graphene sheets. (a) 9-5 defect caused by a single vacancy, (b) 5-8-5 caused by double vacancy, and (c) SEM of a graphene sheet with grown-in defects and defects due to electron irradiation. (reproduced with permission from Banhart *et al*.[31])

2.3 Graphene Properties

2.3.1 Mechanical Properties

Theoretical studies and simulations have indicated that pristine graphene exhibits extraordinary mechanical properties because of its sp^2 hybridization. Graphene's hexagonal lattice allows for the sheet to oppose a variety of in-plane deformations.[32] The mechanical properties of free-standing graphene were first measured by using nanoindentation in an AFM. This technique uses a diamond AFM tip to measure the breaking strength and strain of a graphene monolayer suspended over a silicon wafer

substrate. From these measurements, the Young's modulus was determined to be ~1.0 TPa and the intrinsic tensile strength was ~130 GPa.[19, 32]

2.3.2 Electrical Properties

As mentioned previously, graphene's structure lends itself to outstanding electrical conductivity. The delocalized π bonds, which run across the entire graphene basal plane, allow for electrons to move freely in the plane. Reported values of electrical conductivity and the corresponding resistivity for graphene are 6000 S/cm and 10^{-6} Ωm, respectively.[29]

2.3.3 Thermal Properties

The measured in-plane thermal conductivity of graphene is in the range of 3000-5000 W m^{-1} K^{-1} at room temperature.[33] The heat flow in-plane mainly occurs by phonon transport and phonon-phonon scattering is responsible for the thermal resistance.[34, 35] By contrast, the cross-plane thermal conductivity of graphene at room temperature is a mere 6 Wm^{-1} K^{-1}.[33] The heat flow across the plane is strongly limited by weak inter-plane van der Waals interactions. Interestingly, the cross-plane thermal conductivity does not drastically change with an increase in the number of layers for few-layer graphene samples.

2.3.4 Optical Properties

A single layer of graphene has been experimentally observed to absorb about 2.3% of incident light over a broad wavelength.[36] The absorption of light was found to increase linearly with the addition of a number of layers, with each layer absorbing ~2.3% of incident light. The absorption of light generates electron-hole pairs in the graphene surface which recombine on the order of picoseconds, depending upon the ambient temperature as well as the electron and hole density.[36]

2.3.5 Other Properties

In addition to the extraordinary previously mentioned properties, graphene has a theoretical surface area of 2630 m^2/g.[37] Lab produced graphene sheets measured by Brunauer-Emmett-Teller (BET) are on the range of ~100-1000 m^2/g.[37, 38] BET is used as a marker of nanomaterial dispersion, as BET is an indirect measure of "atoms at surface rather than bulk". Like other dispersions of nanomaterials with high aspect ratios, once removed from the solvent, graphene sheets usually aggregate and restack due to van der Waals interactions between neighboring sheets.[39]

2.4 Characterization Techniques

2.4.1 Atomic Force Microscopy (AFM)

AFM is regarded as the leading approach to measuring sample thickness and determining the number of layers. AFM uses a sharp tip (~5-10 nm) on the end of a cantilever to detect changes in vibration amplitude and frequency in order to create a

topographical profile of the sample.[40] Since the thickness of a pristine graphene sheet is around 0.35 nm, the number of layers can be determined from the sheet thickness.

2.4.2 SEM and TEM

Scanning electron microscopy (SEM) and Transmission electron microscopy (TEM) generally used to visualize the structure and morphology of graphene samples. Defects and folds in the graphene sheets can be seen through these visualization techniques. TEM has the added benefit of being able to determine flake thickness statistics based on folds found in the graphene sheet. (**Figure 5**)

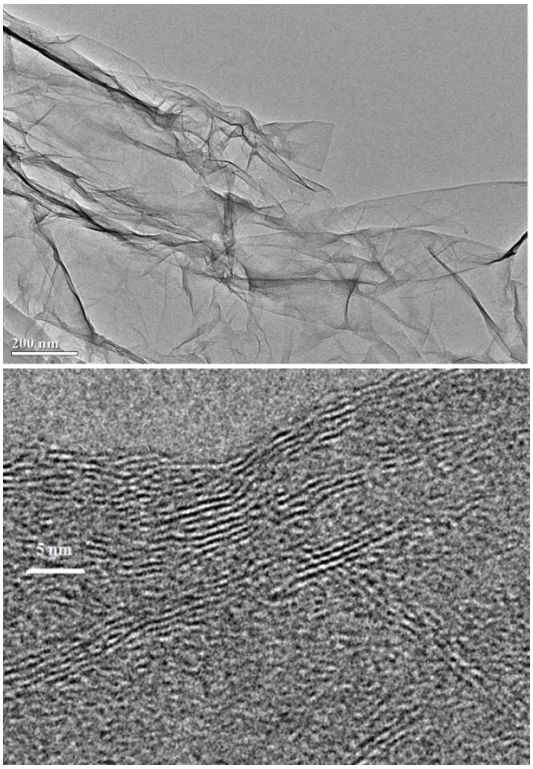

Figure 5: (a) TEM image of graphene showing folds and overlapping sheets, (b) HRTEM image of graphene (reproduced from ACS Material[41])

2.4.3 Raman Spectroscopy

Raman spectroscopy is a vibrational technique that is incredibly sensitive to geometric structure and bonding within molecules.[42] The Raman spectra display a relatively simple structure characterized by two principle bands designated as the G and 2D bands. A third band, the D band may also be present indicating defects within the carbon lattice.

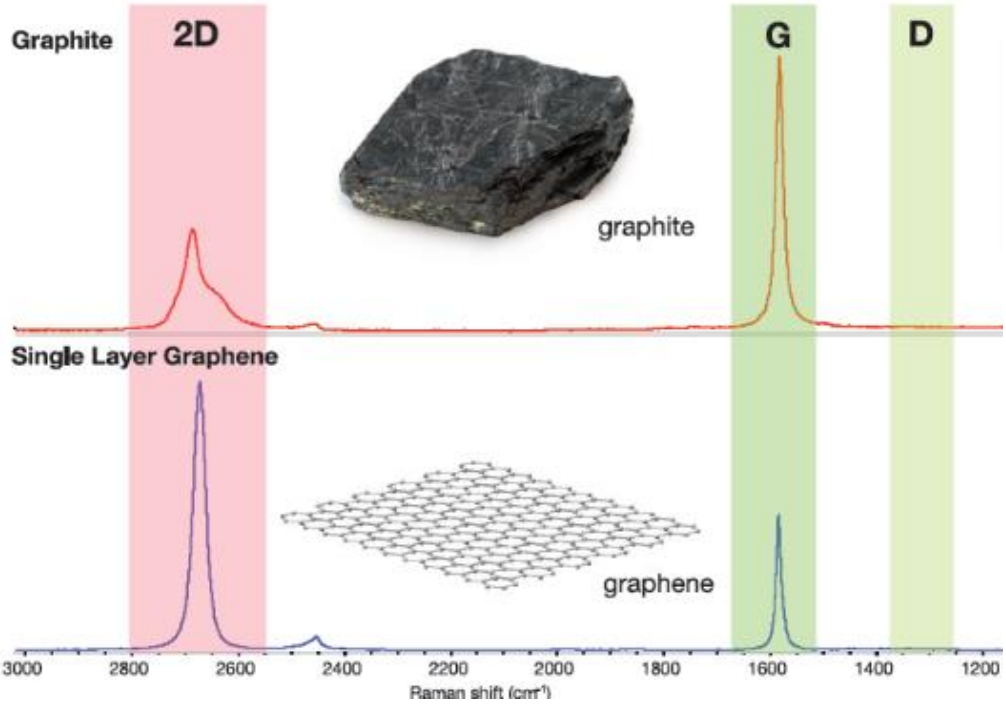

Figure 6: Raman spectra of graphite and single layer graphene, collected with 532 nm excitation. (reproduced from Hall[42])

The G band appears as a sharp peak around 1587 cm^{-1}.[40, 42, 43] The band is an in-plane vibrational mode involving the carbon atoms that are part of the covalent π

network. The G band is sensitive to the number of layers in the sample and is a method to determine the approximate sample thickness. The D band is known as the defect band or the disorder band and can be seen as a peak around 1300 cm^{-1}.[40] In both graphite and graphene, the D peak is weak and will not be noticed on the spectra. However, if the D band is significant, then it means that there are many defects in the material. The 2D band can be observed around 2675 cm^{-1}. The 2D peak can also be used as an indicator of the number of layers present in the sample. Single layer graphene will show a single peak, very similar to a bell curve. An increase in the number of layers will cause the 2D peak to become broader and possibly contain more than one peak in this band. The intensity ratio of the 2D and G bands is very useful in identifying high quality defect free graphene. Single layer graphene has a value of $I_{2D}/I_G = 2$.[42]

2.4.4 X-ray Photoelectron Spectroscopy (XPS)

XPS spectra are obtained from measuring the kinetic energy and the number of electrons that escape the material surface when the material is irradiated with a X-ray beam.[40] XPS is a powerful characterization technique in order to determine elements on the surface of the material. This is important to determine if the graphene sheet has been oxidized or functionalized. It is widely adopted that the sp^2 carbon bond has a binding energy of approximately 284.6 eV. C-O bonds and C=O bonds are around 286 eV and 287 eV, respectively.[40]

2.4.5 Thermogravimetric Analysis (TGA)

TGA is a simple and practical technique to calculate the degree of oxidation of produced graphene samples. TGA measures the mass lost from the sample as it is heated from room temperature to around 1000°C in an inert environment (**Figure 7**). The weight loss up to 120°C is due to the evaporation of water, from 120 to 320°C is the decomposition of labile oxygen groups (i.e carboxyl, anhydride, or lactone groups), and above 320°C is the removal of more stable oxygen groups (i.e. phenol, carbonyl, or quinone).[44]

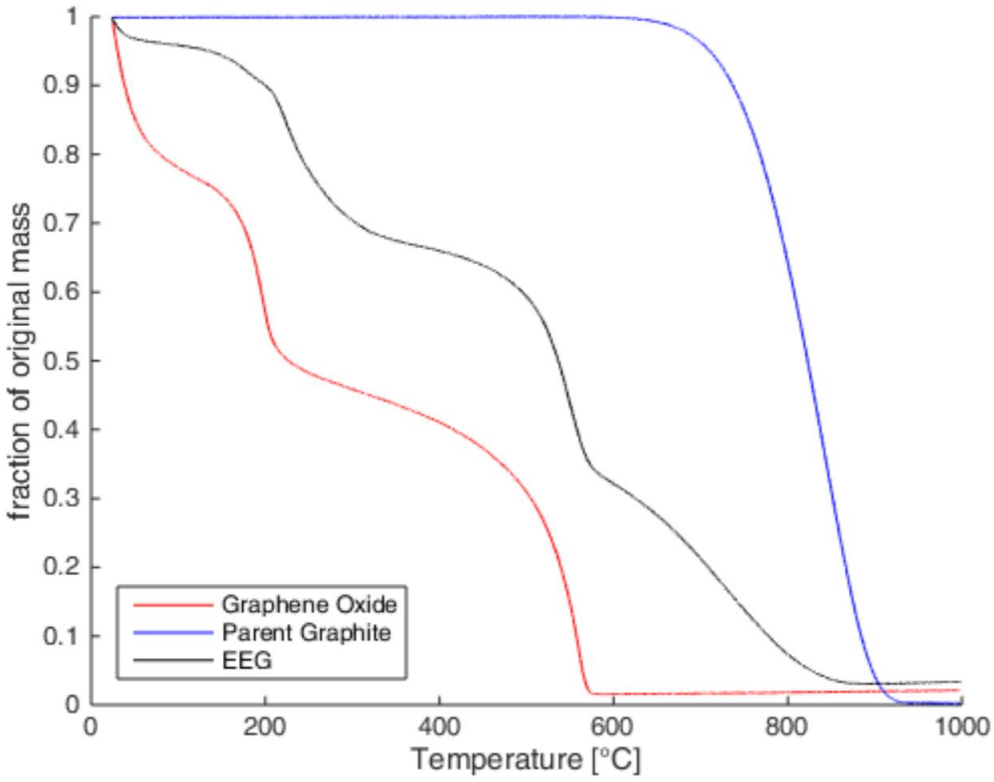

Figure 7: Thermogravimetric Analysis of graphite flakes, graphene oxide produced from modified Hummers' method, and electrochemically exfoliated graphene (EEG). (reproduced with permission from Achee *et al*.[16])

2.4.6 Other Techniques

Brunauer-Emmett-Teller (BET) is a technique used to determine the surface area. The surface area is obtained from nitrogen absorption-desorption so the surface at 77 K.[40] Optical Microscopy can be used to measure graphene sheet lateral size of relatively large flakes, usually on the order of micrometers in length (**Figure 8**).

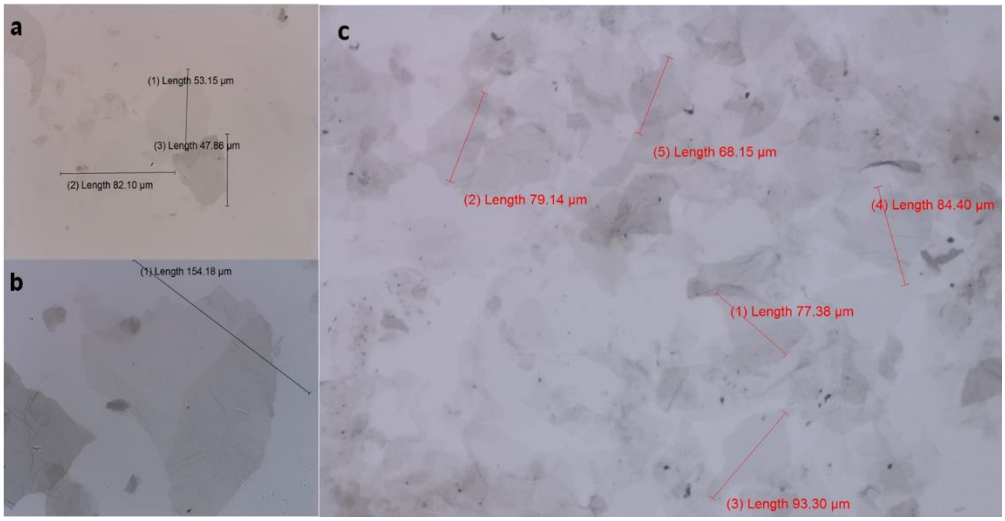

Figure 8: Optical microscopy images of few-layer graphene sheets.(reproduced with permission from Achee *et al.*[16])

2.5. Applications of Graphene

The extraordinary properties of graphene have allowed for a wide range of potential applications.[45, 46] A large portion of this research is into the applications of graphene industries such as electronics, light processing, energy storage, and supercapacitors[7-13] With a material that is as unique as graphene with such remarkable properties, graphene is set to become the wonder material of the 21st century.

2.5.1 Electronics

With miniaturization driving the electronics industry, graphene's ability to remain stable at thin levels coupled with high conductivity at room temperature has drawn enormous attention. In the telecommunications sector, graphene-silicon hybrids have already shown, through prototypes, to be more efficient than current silicon phase modulators. This allows for larger packages of data to be transferred at much higher rates. These hybrid phase modulators would theoretically have lower optical losses, reduced energy consumption, and error-free bit operation for up to 50km.[47, 48] Long term, silicon circuits would fully transition over to graphene.

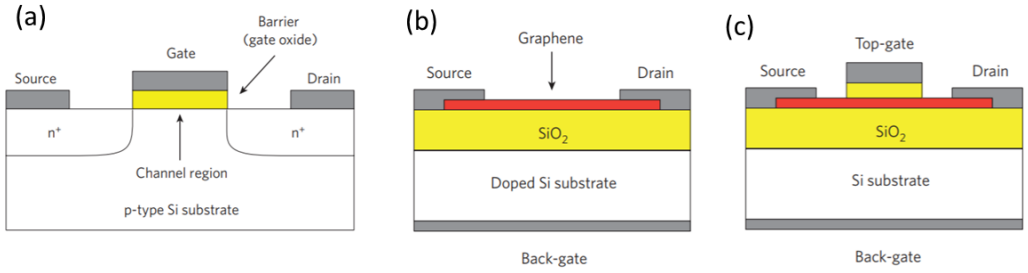

Figure 9: Cross-sections of MOSFETs. (a) A conventional n-channel Si MOSFET, (b) back-gated graphene MOSFET, (c) top-gated MOSFET with a channel of graphene. (reproduced with permission from Schwierz[49])

2.5.2 Solar cells and energy conversion

Graphene's unique properties, including high surface area, large electrical conductivity, chemical stability, high mechanical flexibility, and light weight nature, is projected to play a key role in meeting the demand in both energy generation and

storage.[50] Notably, perovskite solar cells have been plagued with poor interface between layers, leading to charge recombination, ion diffusion, and short circuits.[50] Graphene has been used to increase the interface properties of high-performance perovskite-based solar cells through the use of interface engineering.[50, 51]

2.5.3 Supercapacitors

Supercapacitors or ultracapacitors have attracted world-wide attention due to their high power density, high charge/discharge rates, and long cycling life.[52-54] They have the potential to complement or replace the batteries for energy storage applications, especially in wearable and/or portable electronics and electrical and hybrid vehicles.[55] Based on the energy storage mechanism, supercapacitors can be classified into to two main categories: electrical double layer capacitors (EDLCs) and pseudocapacitors.[56] For EDLCs, the capacitance originates from the accumulation of charges at the electrode-electrolyte interfaces. Carbon-based materials, such as active carbon, graphene, reduced graphene oxide, and carbon nanotubes (CNTs), are widely used in the electrodes of EDLCs. [56-59] Considering there are no chemical reactions involved during the charging/discharging in EDLCs, the cycling life is impressive, but the specific capacitance is limited. Optimizing specific surface area and pore size, and improving electrical conductivity are the effective approaches to achieve a high capacitance and energy density.[60] As for the pseudocapacitors, the energy storage is from the faradic charges between electrolyte and electrode based the reversible redox reactions, which usually show a higher specific capacitance and energy density.[61-63] Usually, transitional metal oxides (MnO_2, MoO_3, and RuO_2) and conductive polymers (polyanilines and polypyrroles)

are utilized for pseudocapacitors.[64-68] However, the relatively poor electrical conductivity is a major drawback of the active materials in pseudocapacitive, resulting in short cycling life.

Graphene's high surface area and electrical conductivity enable graphene to be widely used in supercapacitors, especially EDLCs. For example, a theoretical specific capacitance of 550 F/g could be achieved if the surface area of the electrode could be fully utilized with single-layer-graphene. However, the real specific capacitance of a graphene-based supercapacitors is much lower than the theoretical value. This can be due to defects in the material or the agglomeration of sheets during graphene synthesis and electrode preparation.

CHAPTER III

GRAPHENE PRODUCTION REVIEW AND FIRST-GENERATION REACTOR

3.1. Graphene production overview

Depending on the production method of graphene, the structure and hence quality will depend heavily on the graphitic precursor. There are two different approaches for producing graphene:

- Top-down approach – transforming graphite into graphene by overcoming the van der Waals forces between layers. Top-down approaches have shown significant interest as it is the primary source of mass-produced graphene. While these approaches will not guarantee large lateral size and pristine single-layer graphene, they will meet the needs of most graphene applications in the near future. Top-down approaches use graphite as a precursor, which is a crystalline material that is essentially constructed from multiple graphene sheets with an interplanar spacing of 0.355 nm.
- Bottom-up approach – building of graphene sheets from molecular carbon building blocks. Bottom-up techniques involve the utilization of chemical reactions to produce 2-D graphene from hydrocarbon precursors. Bottom-up approaches have shown to produce large defect-free single-layer graphene sheets. However, these approaches have their drawbacks. They are slow

processes and will not meet the world-wide demand for graphene. They also require large amounts of energy and are limited by the processing technology.

For methods that start with graphite in the form of graphite foil or graphite flakes, the crystallinity of the graphite will be important, as graphite is a polycrystalline material. Like all crystalline materials, graphite is subject to defects such as edge dislocations and twinning (**Figure 10**).[69] However, since the graphite layers are held together by van der Waals forces, there are no screw dislocations. Fewer defects in the parent graphite will allow for higher quality graphene to be produced.

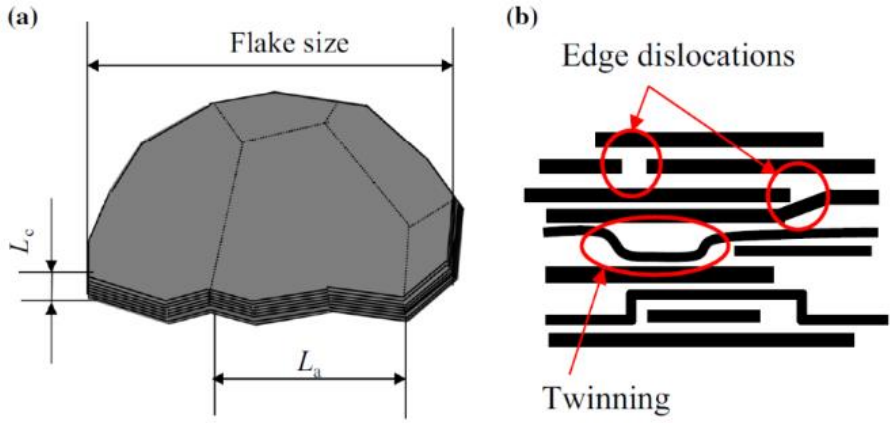

Figure 10: (a) Top-down view of grain boundaries on a graphite flake will remain present on the graphene sheet produced from this material. (b) Side view of stacking defects found in graphite flakes (reproduced with permission from Mori *et al.*[69])

In the past decade, top-down and bottom-up approaches have been used to create graphene for various applications. While both bottom-up and top-down approaches have shown to be better fit to certain desired qualities, this thesis will focus on top-down methods as it is the most promising to commercial scale graphene production. **Figure 11** depicts important considerations when designing a large-scale top-down graphene production method. Each method described in the following sections will produce various grades of graphene that may be better suited for a specific application.

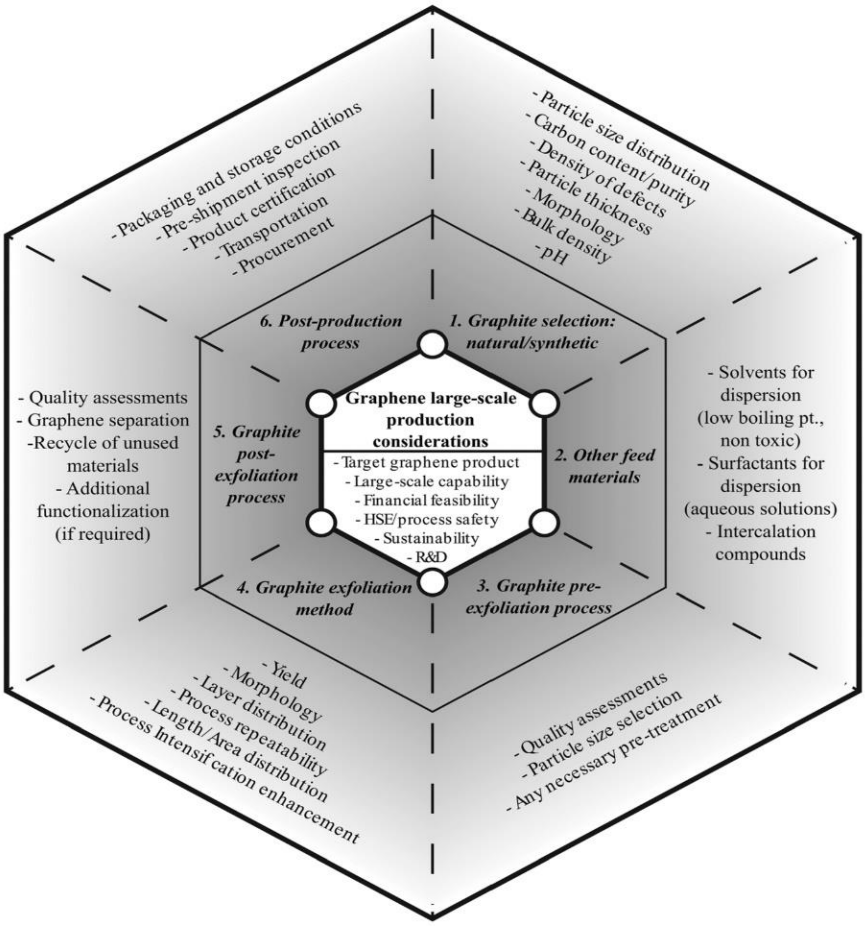

Figure 11: Large-scale graphene production considerations for top-down methods. (reproduced with permission from Stafford *et al.*[14])

3.2. Graphene Oxides and Derivatives

3.2.1 Graphene Oxide Synthesis

Graphene oxide (GO) has long been used as a precursor to graphene. GO is a highly oxidized form of graphene in which the edges and basal plane are heavily functionalized with oxygen-containing groups.[28] GO is produced by the oxidation of graphite to form graphite oxide, followed by exfoliation of the graphite oxide to form GO. The oxidation is typically caused by chemical treatment in the presence of strong oxidizing agents such as H_2SO_4, HNO_3, H_3PO_4, $KClO_3$, and $KMnO_4$, to intercalate and exfoliate the graphite parent material.[30, 70, 71] This will form carbonyl, hydroxyl, or phenol groups on the graphene sheet (**Figure 12**).[28, 30, 72-74]

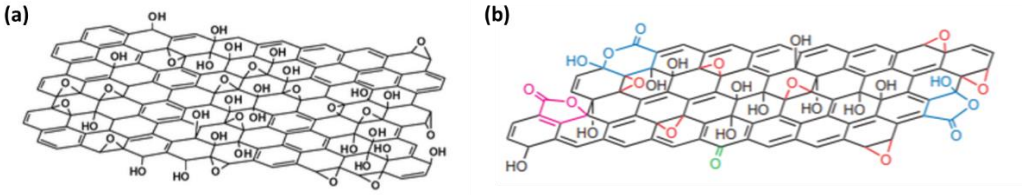

Figure 12: Proposed structures of GO: a) GO functionalization based on Lerf-Klinowski model (reproduced from Dreyer *et al.*[30]), b) GO structure containing lactol rings at edges (reproduced with permission from Gao *et al.*[75])

One of the earliest methods to produce graphene was through a modification of Hummers' Method. The original Hummers' method was used to produce graphitic oxide.[76] However, this can be modified to produce graphene oxide through the use of sonication.[77] Hummers' method uses concentrated sulfuric acid with potassium permanganate and sodium nitrate acting as catalysts.[76] The graphite oxide can then be

exfoliated using bath sonication or ultrasonication in order to produce graphene oxide of a few layers, typically 3-5 layers.[30, 71, 76]

While Hummers' method produces large quantities of GO, this is uses very harsh acids and requires long durations of washing in order to remove the acid from the final product. This hinders the scalability of the process and is not environmentally friendly. It has already been shown that at lab scale levels, the process is prone to thermal runaway and explosions. In 2016, two students were hospitalized and another was injured at the Songjiang District campus of Donghua University after the reaction went wrong and caused an explosion that splashed strong acids over the students.[78]

The properties of GO are inferior in comparison to pristine graphene due to distortions in the lattice in the form of sp^3 carbons, holes, and impurities.[72, 75, 79] Using an AFM nanoindentation technique similar to that used for pristine graphene, Gomez-Navarro *et al.* measured the Young's modulus to be ~250 GPa.[80] Due to the surface functionalization of the sheets, the thickness of GO (0.7-1.0 nm) is higher than pristine graphene (0.34 nm).[81]

3.2.2. Reduced Graphene Oxide

Reduced graphene oxide (rGO) is graphene oxide that has been chemically or thermally reduced. This allows for the oxygen groups to be removed from the graphene sheet and the sp^2 network can be partially restored.[74, 82] The highly oxidized GO can then be thermally reduced in an oven at 1000°C. However, some oxygen functional

groups will remain bonded to the graphene sheet and some of the groups that were removed may be replaced with vacancies (**Figure 13**).

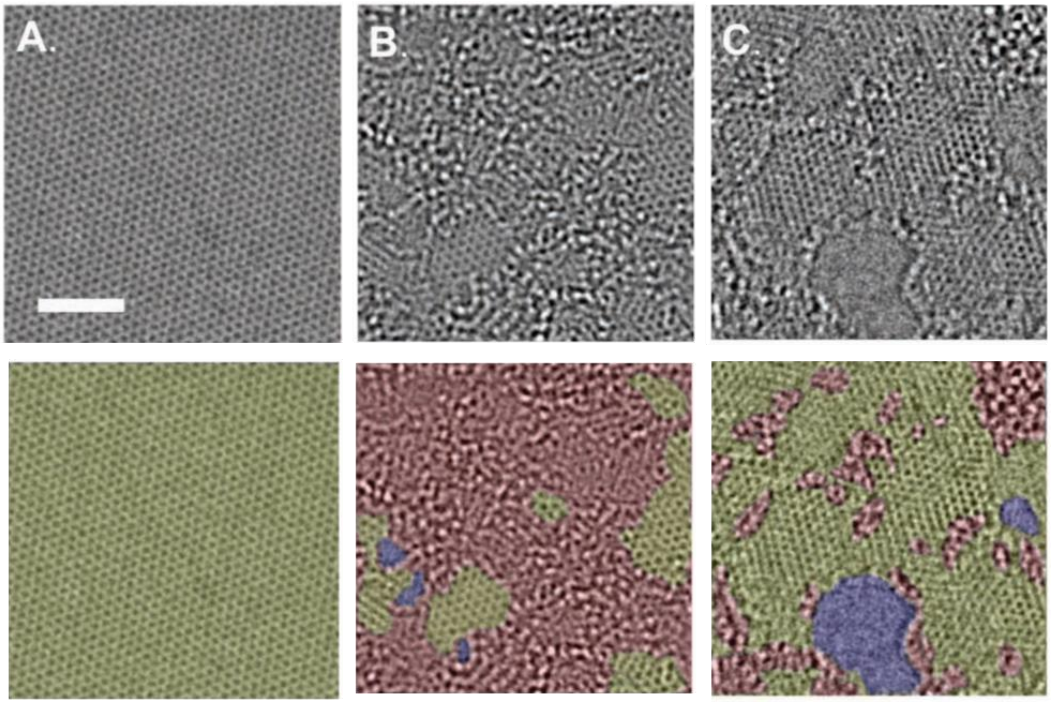

Figure 13: TEM images of (a) Pristine graphene, (b) GO, and (c) rGO. Scale bar, denoting 2 nm, is valid for all images. The graphitic area is indicated in yellow, the oxidized regions are in red, and holes are indicated in blue. (reproduced with permission from Erickson *et al.*[74])

These impurities and defects act as charge concentrations and scattering sites, thus causing the unique properties to be impaired compared to pristine graphene. The properties of rGO are highly dependent on the initial oxidation level of GO, reduction method, and the extent of reduction. Reduction of GO helps to restore the sp2 bonding network, but the residual sp3 functionalized carbons and atomic defects will act as scattering sites and hinder ballistic transport.[83-85] The Young's modulus of typical rGO sheets are in the range of 185-250 GPa, which is more similar to that of GO.[86]

3.3. Pristine Graphene Production

3.3.1. Liquid Phase Exfoliation with Sonication, Solvent Matching, and Surfactants

In order to produce single layer graphene sheets from this graphite parent material, the critical exfoliation energy van der Waals forces between the graphene sheet must be overcome. Another issue that arises once the sheets are exfoliated is to avoid restacking of the sheets. This can be done by minimizing the interaction between the sheets through the use of solvents or aqueous surfactant solutions, such as cyclopentane (CPO) and N-Methyl-Pyrrolidone (NMP) or sodium dodecylbenzene sulfonate (SDBS), respectively.[14]

3.3.1.1 Liquid Phase Exfoliation with Shear

A viscous fluid would be transported through the device in-between the cylinder walls of a shear mixer or Taylor-Couette device. The rotation of the cylinder walls applies a shear force on the graphite and causes the layers to be mechanically exfoliated when a suitable force is applied to overcome the van der Waals forces between the adjacent layers (**Figure 14**). Paton *et al*. showed that any device that can achieve a minimum shear rate of $10^4 s^{-1}$ will be able to exfoliate graphite.[87] In order to help create a continuous process that can be used to create a relatively high yield, the graphite would suspend in a liquid phase that allows for the graphite to flow through the small gap in the reactor and the graphite would be stabilized using a solvent such as NMP to reduce the effects of aggregation and restacking.[87-89] Due to the prolonged shear forces that the graphite experiences as it travels down the Taylor-Couette reactor causes the graphite undergoes a fragmentation mechanism. [14] This causes the graphite lateral size to drop to the

between the 500 to 1500 nm range. The final product lateral size range will vary based on the precursor graphite that is used, the length of the reactor, and the shear rate that the graphite solution experiences. However, the AFM showed that the produced graphene was indeed 0.6 to 3 nm thick, 2-10 layers, corresponding to few-layer graphene sheets. The Raman spectroscopy showed that the produced graphene had a low degree of defects, as evident of an I_D/I_G ratio of ~0.14, and the XPS showed that the flakes were not oxidized, confirming the high quality of these flakes.[14]

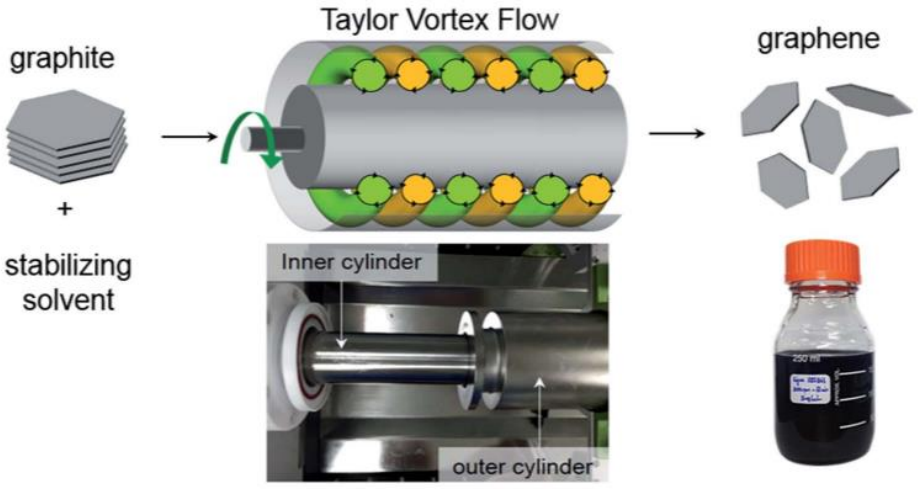

Figure 14: Schematic depicting the process of shear-exfoliation of graphite into few-layer graphene by a Taylor Vortex device. (reproduced from Tran *et al.*[90])

3.3.1.2 Liquid Phase Exfoliation with Solvent Matching and Surfactants

In order to produce graphene from graphite, the van der Waals forces between sheets must be overcome. Another method of achieving this is by increasing the interfacial tensions between the solid and liquid. Higher interfacial tensions between the solid and liquid leads to decreased dispersibility of the solid in the liquid.[91] Surfactants

have shown to improve exfoliation efficiency of graphene exfoliation in organic solvents. Organic salts like edetate disodium, potassium sodium tartrate, and sodium tartrate have shown to be excellent surfactants for direct exfoliation in organic solvents such as NMP, DMF, and DMSO.[92]

3.3.2 Electrochemical Exfoliation

The graphite, typically graphite foil, is placed into an electrolyte bath and connected to a power source. A voltage is then passed through the graphite foil and allows for the electrolyte solution to intercalate into the graphite foil. The use of an applied voltage allows for weaker acids to be used for intercalation and exfoliation.[16, 93] For anodic electrochemical exfoliation, an inorganic aqueous electrolyte solution is used, such sulfuric acid. Once the electrolyte has intercalated between the graphene layers, the voltage allows for the following electrochemical reaction:

$$SO_4^{2-}(l) \rightarrow SO_2(g) + O_2(g) + 2e^- \qquad (1)$$

$$2H_2O(l) \rightarrow O_2(g) + 4H^+ + 4e^- \qquad (2)$$

The transformation of the sulfate ions and water into gaseous sulfur dioxide and oxygen inside the graphene layers causes the graphite to form an accordion shaped expanded graphite.[16] The expanded graphite can then be exfoliated through more traditional mechanical exfoliation mechanisms, such as shear mixing or tip sonication. The use of the electrolyte solution does cause some oxidation of the produced graphene, but it is significantly less than that of purely chemical exfoliation. The Raman I_D/I_G ratio is

about 0.25 and the layer thickness can vary from monolayer to multilayer graphene (MLG).[14, 94]

3.4. First-generation Reactor: Electrochemical Containment Exfoliation

3.4.1 Limitations of Electrochemical Exfoliation

While electrochemical exfoliation of graphite rods has proven to produce few-layer graphene with a large lateral size and fairly low defects, there are still some major drawbacks to this method. The graphite rod must maintain direct electrical contact to the power source in order for there to be a significant exfoliation yield. Once the graphite foil begins to exfoliate, the suspended graphite rod monolith disintegrates and falls to the bottom of the system. Liu *et al.* attempted to address this challenge by placing the graphite electrode at the bottom of the exfoliation reactor with the expectation that gravity would allow for the disintegrated graphite particles to remain connected.[95] They reported slight improvements, but process is very slow and can lead to poor aspect ratio distributions of the produced graphene if completed too quickly or an increase in the oxidation of the graphene if the process is too slow. Kinloch *et al.* proposed a continuous reactor method in which the graphite foil would be pushed up through the bottom of the reactor to be exfoliated (**Figure 15)**.[16, 96] This method allows for the graphite that has expanded to few-layer graphene to still maintain electrical contact and continue the intercalation/exfoliation process.

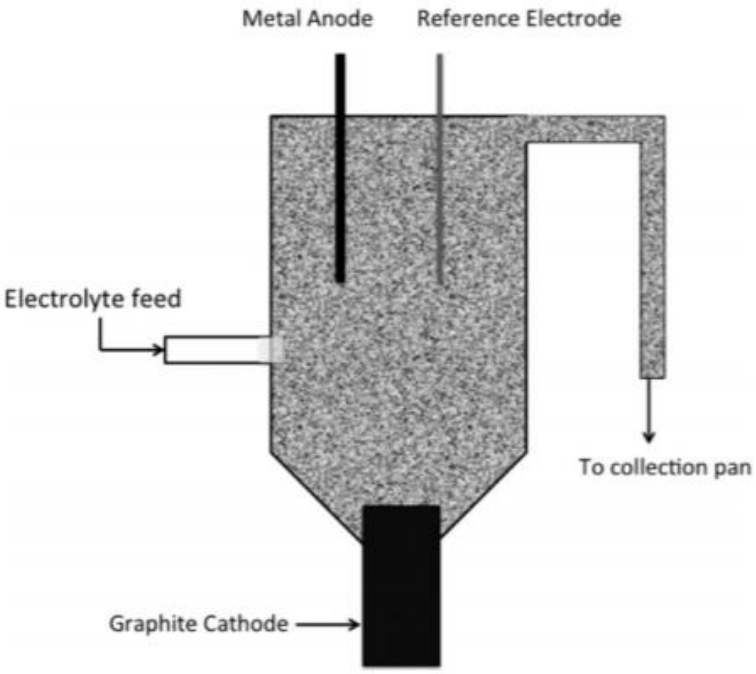

Figure 15: Schematic of an electrochemical cell for a continuous process using graphite foil. (reproduced with permission from Abdelkader *et al.*[96])

3.4.2 First-generation Reactor

Despite these advances in electrochemical exfoliation, there are a number of major challenges facing the field: (i) Only graphite monoliths, not powders, may be used as a source for electrochemical exfoliation because the graphite electrode must be continuous, electrically conductive, and connected to the external wire. (ii) Most importantly, if electrochemical exfoliation actually occurs and the monolith is expanded to form graphene, then the monolith disintegrates and the electrochemical exfoliation process stops. The graphite electrode tends to fall apart as intercalation proceeds, and when graphite pieces become disconnected from the monolith (and thus, the circuit), they can no longer participate in the intercalation process. These fallen pieces are a mixture of unexfoliated graphitic particles and graphene.

Our method overcomes these various problems and provides a new mechanism for one-step, scalable, high-yield graphene powder production. We emphasized the production of graphene powder (rather than colloidal dispersions) because this form of graphene is directly applicable both as an additive in polymer composite applications and in battery or supercapacitor electrodes.[97-99] The graphene powder produced through this method is termed as electrochemical exfoliated graphene (EEG).

The concept demonstrated by our group in Achee *et al.* suggests that adding a compressive force to the partially exfoliated graphite will not only increase the exfoliation rate, but will also allow for a more uniform aspect ratio distribution of the produced graphene sheets as compared to graphite foil electrochemical exfoliation reactions.[16, 100] **Figure 16** shows the setup for electrochemical containment exfoliation.[16] Rather than a monolithic graphite rod electrode, graphite flake powder was confined inside a permeable, expandable container. The graphite powder is compressed together to yield a conductive working electrode. The compression within the system is sufficiently high to maintain graphite connectivity, but the system also expands with the expanding graphite sample. A platinum wire (the current collector) is inserted in the container and connected to graphite powder. A separate conductive plate functions as a counter electrode. The compressed graphite working electrode and the counter electrode are both immersed in an aqueous electrolyte (0.1 M $(NH_4)_2SO_4$). A positive voltage (+10 V) is applied to the graphite electrode. The graphite is intercalated with sulfate and continuously expands over time. Because of the compression of the bag, the powder remains in electrical contact, even as it expands due to intercalation.

Using graphite flakes as compared to graphite foil has the benefit of increasing the total surface area that is available for expansion and exfoliation. For graphite foils, the reaction only occurs at the surface of the material, whereas for a graphite flake bed, the electrolyte can diffuse through the graphite flake bed and react with materials on the inside of the bed. Using graphite flakes significantly increases the graphitic surface area available for exfoliation. Additionally, graphite foil can introduce impurities in the form of acid treatment during the process of forming graphite foil or the use of binders. This acid treatment can functionalize the graphite and increase wettability to electrolyte, which increases the yield.

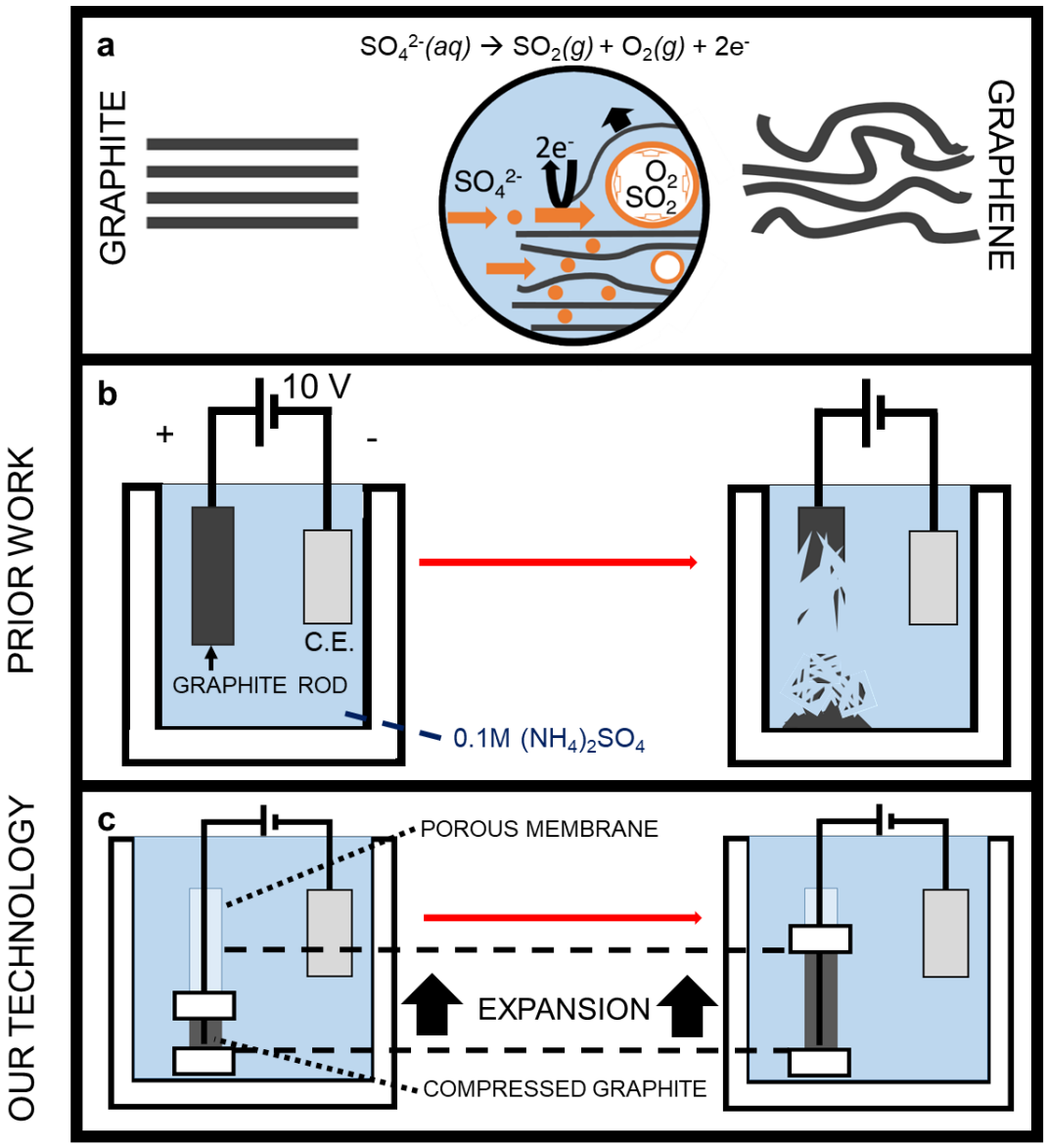

Figure 16: Schematic showing the intercalation mechanism for electrochemical exfoliation as well as the idea behind electrochemical containment exfoliation. (reproduced with permission from Achee *et al.*[16])

3.4.3 Characterization of Produced Graphene

AFM was utilized to determine that the thickness of the graphene sheets was between 2-7nm (**Figure 17a,b**). Raman spectroscopy with a 532-nm excitation laser was used on EEG on a glass slide. The ratio of D peak to G peak (ID/IG) varies from 0.9 to 1.2 in different spots. Typically, an ID/IG ratio of 1.2 is very similar to chemically or thermally reduced GO (~1.1–1.5)[101]. The symmetric 2D peak of our EEG is quite similar to previously reported few-layered graphene (**Figure 17e**). XPS was used to probe the chemical composition of the EEG (**Figure 17f–h**) (no shear mixing). The EEG shows 16.7 atom % oxygen content. The corresponding C/O ratio of 4.98 for EEG is significantly lower than prior work on electrochemically exfoliated graphene, suggesting a higher degree of oxidation of the parent graphite during the electrochemical exfoliation process[3]. This occurs because our process is not arrested by the disintegration of the graphite electrode, in contrast to prior studies. The EEG shows less oxygen functional groups than GO from Hummers' method, but more oxygen functional groups than thoroughly thermal-reduced graphene oxide. This means our EEG has similar chemical/surface properties to partially reduced graphene oxide.

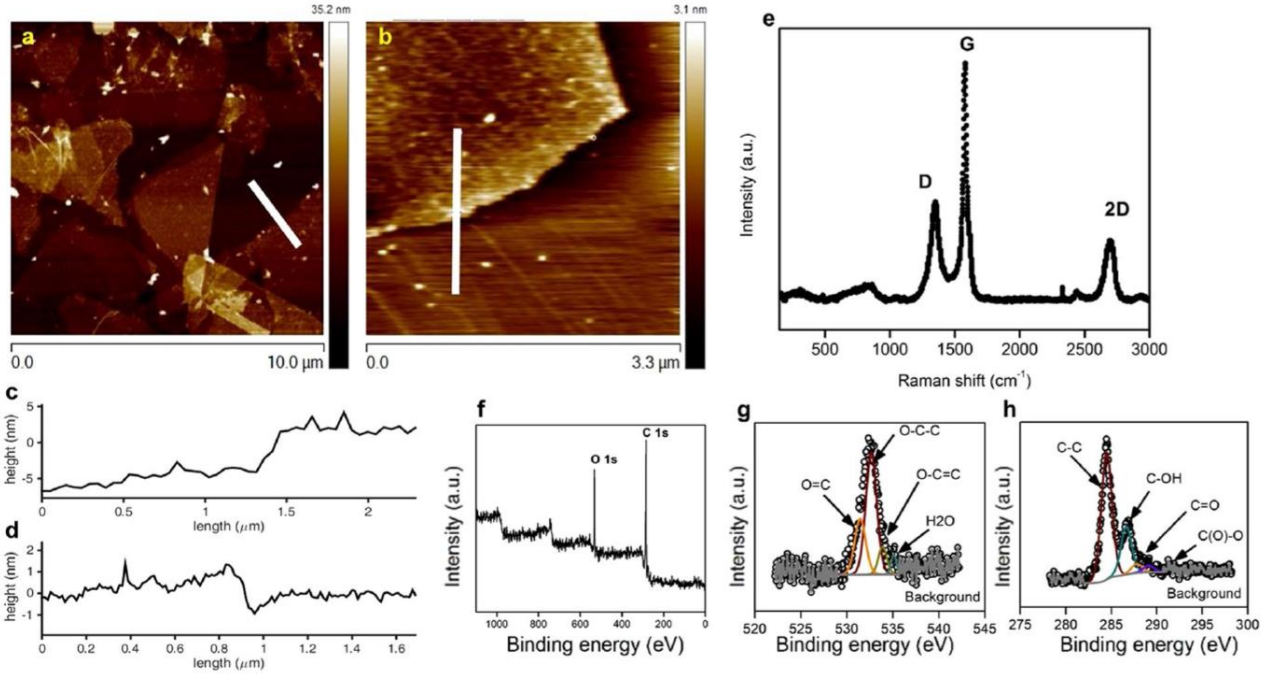

Figure 17: (a,b) AFM topography of graphene sheets, (c,d) height mapping of graphene, (e) Raman spectra, (f-h) XPS.(reproduced with permission from Achee *et al.*[16])

CHAPTER IV

SECOND-GENERATION ELECTROCHEMICAL EXFOLIATION REACTOR: SCALABILITY AND LIMITATIONS

4.1 Experimental Setup and Methods

4.1.1 Second-generation Reactor

Expanding upon the work of Achee *et al*, the electrochemical containment exfoliation had an external weight added in order to ensure compression of the graphite bed so that it remains as a conductive monolith during the reaction.[16, 100] The reactor size was also increased to show potential scalability and amplify parameters that may cause a limitation to the reaction.

The pre-treatment process increases the wettability of the parent graphite material by functionalizing the graphite flakes along the edge and enhance the intercalation and exfoliation process in the reactor.[16] The washing step removes residual nitric acid from the graphite flake solution before being added to the reactor. The flake pre-treated graphite flakes are placed into a permeable membrane and placed under a weight to maintain electrical contact throughout the entire reaction process. The entire setup is completely submerged in an electrolyte bath of 0.1M ammonium sulfate.

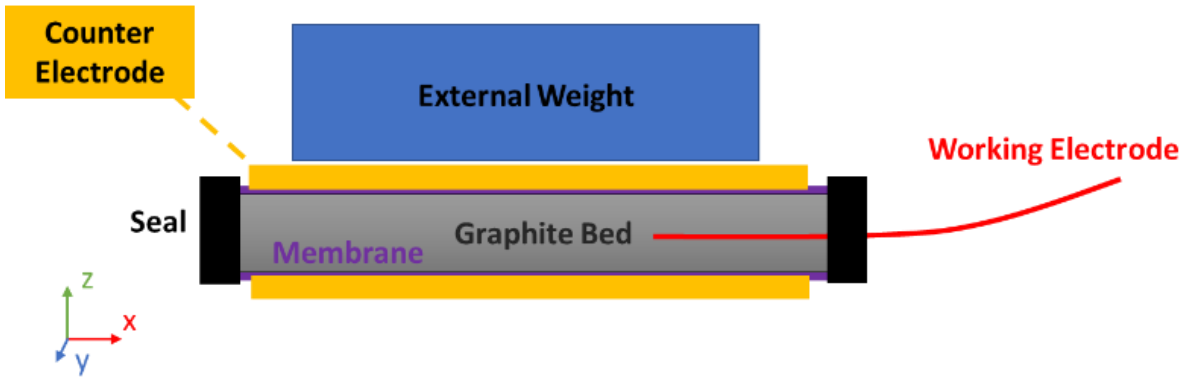

Figure 18: Schematic of electrochemical containment exfoliation reactor.

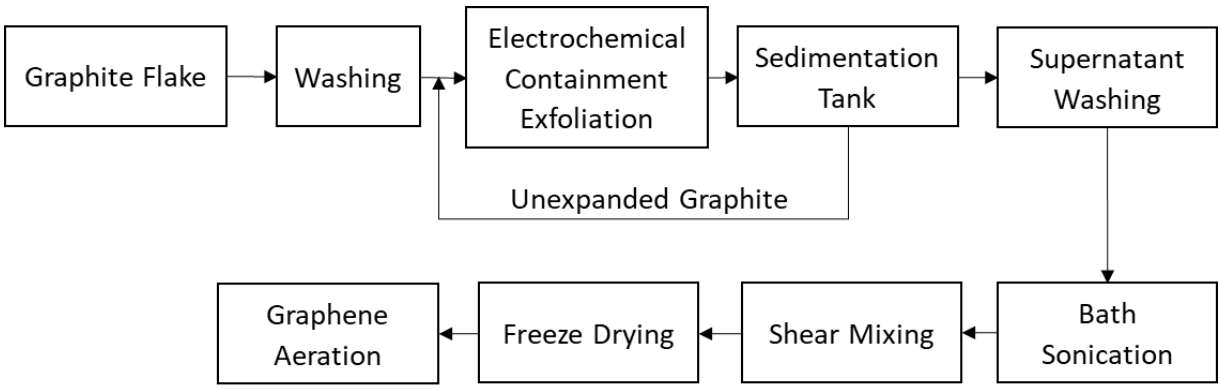

Figure 19: Block flow diagram for the front-end process of electrochemical containment exfoliation.

In our work, the graphite flakes are compacted into a tubular cellulose dialysis membrane (MEMBRA-CEL MD77) and sealed the bag at one end and a movable clip on the other end.[16, 100] The movable clip at the end of the dialysis membrane is used to compact the graphite flakes into an electrically conductive monolith but also allows for expansion of the graphite flakes within the dialysis bag as the reaction progresses. A platinum 18 gauge wire was inserted into the permeable container so as to connect the graphite flakes to the power source (Acopian Power Supply Model Y0135LXB530). The counter electrode (current collector) used in these experiments was a graphite foil sheet. However, other conductive, non-reactive materials such as platinum or stainless steel could be used. The working electrode (platinum wire and graphite flake bed) and counter electrode are both submerged in an aqueous electrolyte. When a positive voltage of 10V is applied to the system, the graphite flakes are exfoliated through a cyclic process of electrolyte intercalation and expansion.

After completing the reaction, the graphite-graphene slurry is transferred to a sedimentation tank where the unexfoliated graphite crashes out of solution and is collected as sediment on the bottom. The graphene stays suspended in solution and can be collected for post-treatment, which includes shear mixing and freeze-drying to form a graphene powder. Characterization was performed on the produced graphene samples to verify that the material was indeed graphene.

4.1.2 Supercapacitor

A two-electrode Swagelok® stainless steel cell with stainless steel pistons/cylinders was used for quantitative electrochemical characterizations of EEG and

other commercial graphene powders (ACS Material®, Knano®, and Graphene Supermarket®) (**Figure 20**). Platinum disks were placed onto stainless steel current collectors to decrease the contact resistance at the graphene/cylinder interface. A Celgard separator (3501 Coated PP, Celgard LLC, Charlotte, NC) was used. The electrolyte is 1 M H_2SO_4. The working and counter electrode were prepared as following: (1) the graphene powder was mixed well with PTFE (Dupont de Nemours) and active carbon at a weight ratio of 8:1:1 in 20 mL ethanol under magnetic stirring. (2) The mixture was then heated up in oil bath at 70 °C to evaporate ethanol with constant stirring. (3) Afterwards, the solid mixture was rolled to a very thin film and punched into several pieces of circle of 8 mm in diameter. All the thin electrode films have a similar thickness of ~0.2 mm.

The electrochemical testing was performed with a Gamry Reference 3000 potentiostat. From cyclic voltammetry (CV) curve, the specific capacitance (F/g) was calculated based on the equation

$$C = 2\oint_{V_1}^{V_2} \frac{IdV}{v \times \Delta V \times m}, \qquad (3)$$

where V_1,V_2 are the low-voltage cutoff (V_1) and high-voltage cutoff (V_2), respectively; I is the current (A), v is scan rate (V/s), ΔV is the potential window (V), and m is the mass of two electrodes (g).

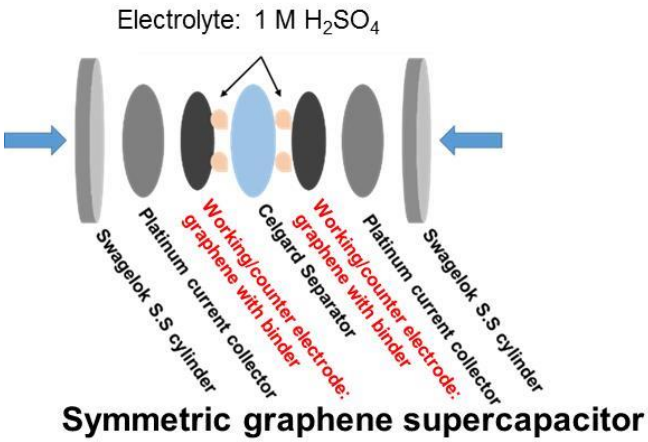

Figure 20: Schematic of a supercapacitor structure based on graphene.

4.2 Results

4.2.1 Diffusion Limitations

In scaling the width (y-dimension) of the reactor, it became apparent that electrical contact was broken if the graphite did not create a continuous uniform bed in the reactor. If too much graphite was added to the reactor, then the electrolyte was not able to pass through the entire packed graphite bed. This is best seen by a variation in the graphite bed thickness.

$$Bed\ Thickness = \frac{\frac{mass\ of\ graphite}{density\ of\ graphite}}{(reactor\ length)*(reactor\ width)} \quad (4)$$

The diffusion limitations could be seen in a cross-section of the reacted graphite bed. A boundary between the parent graphite and the expanded graphene is created.

The parent graphite still maintained its metallic appearance, whereas the expanded graphene appeared as a black sponge (**Figure 21**).

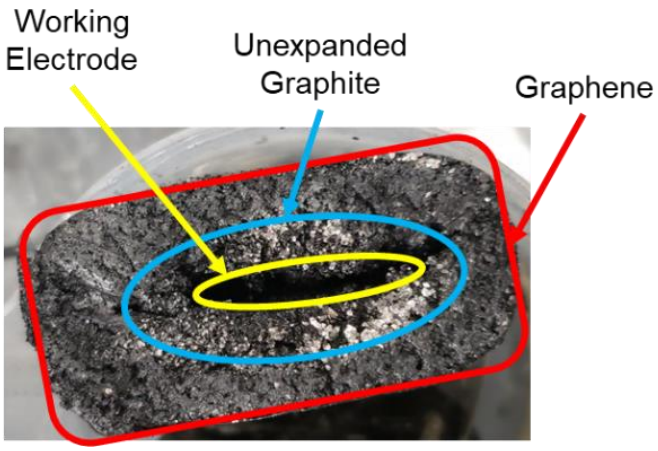

Figure 21: Cross-section of packed graphite bed after 24-hour reaction time.

Poor electrical contact was noted as no current or low voltage (below 10V) passing through the system. However, if the thickness of the graphite bed was increased beyond approximately 0.8 cm, then the reaction was limited by the ability of the electrolyte solution to pass through the packed graphite bed. Within the bed thickness of approximately 0.5-0.8 cm was shown to have a good electrical connection to the graphite bed and also reduce the limitations caused by diffusion of the electrolyte.

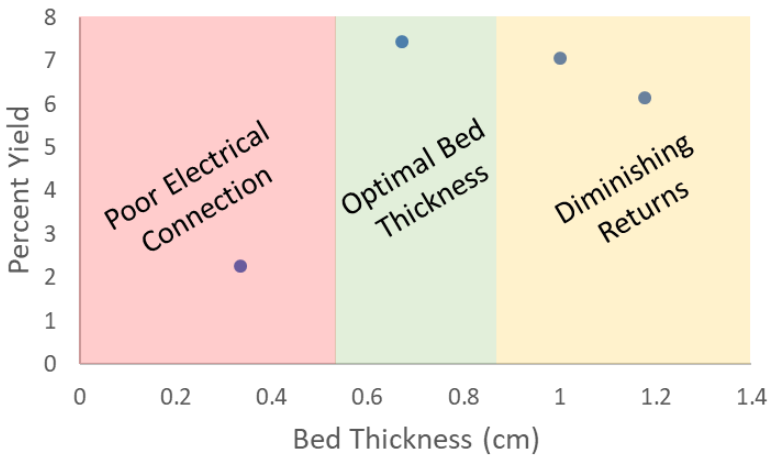

Figure 22: Regions depicting limitations of the reaction based on the dominating factor.

4.2.2 Reaction Kinetics

The production rate of the graphene sheets is very important in determining the viability of commercialization. Production rate is directly correlated to the size of the reactor and the reaction rate. Our prior work in Achee *et al*. has shown that the reactor can be increased in size without changing the quality of the produced graphene. The production rate can be determined from the percent yield of graphene after various reaction times. **Table 1** shows the percent yield, volume percent expansion, and mean lateral size of produced graphene at designated reaction times.

Table 1: Collected metrics from 5g batches of pretreated graphite flakes.

Time (min)	Volume Percent Expansion	Yield	Mean Lateral Size (μm)
5	155%	0%	NA
15	171%	2%	48.2
30	186%	12%	47.2
60	347%	15%	46.9
120	354%	24%	42.6
240	457%	43%	47.5
360	Membrane Rupture	43%	47.3

The volume percent expansion is calculated based on the total volume of the graphite and graphene in the membrane after the reaction (V_1) and the initial volume of graphite that was inserted into the bag (V_0).

$$\text{Volume Percent Expansion} = \frac{V_1}{V_0} \qquad (5)$$

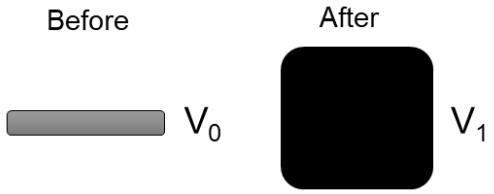

Figure 23: Schematic describing how the volume percent expansion was calculated.

As the reaction time increases, there is a positive trend in the volume percent expansion and amount graphene that is produced. During the first 30 minutes of reaction, the reaction progresses quickly. After the initial 30 min, the reaction slows but continues in a positive linear trend. Since production rate is the derivative of produced graphene mass per time, the optimal production rate of graphene is within the first ~30 minutes of reaction (**Figure 24**).

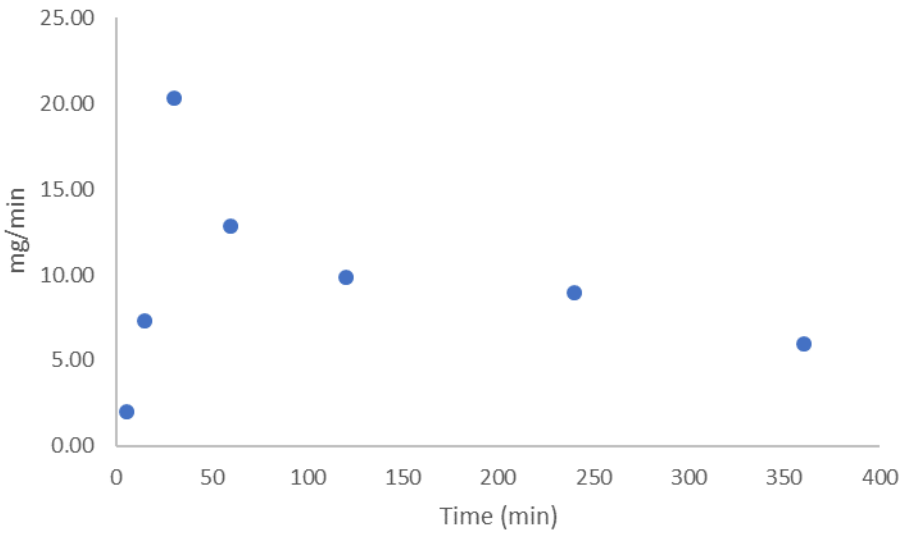

Figure 24: Produced graphene throughput as a function of the reaction time.

4.2.3 Supercapacitor

The CV curves (at a scan rate of 50 mV/s) of supercapacitors based on the tested graphene powders are shown in **Figure 25**. It is clear that the supercapacitor based on EEG has more pronounced rectangular shape than the others, implying the more supercapacitor behavior of EEG. The SEM and AFM images of EEG show the high aspect ratio of EEG. Meanwhile, the very sharp cut-off of EEG curves implies the highest electrical conductivity of EEG, compared to the ones of other commercial graphene.

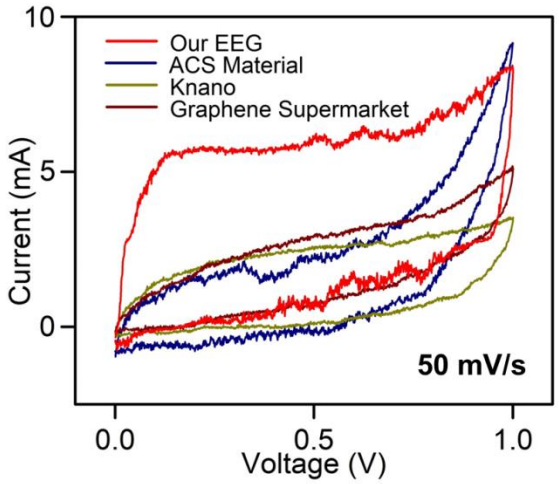

Figure 25: CV curves of symmetric supercapacitors based on EEG and other commercial graphene

The CV curves of EEG from different scan rates are also investigated (**Figure 26**). It is obvious that the EEG could maintain the rectangular shape of CV curves at very high scan rates (up to 500 mV/s). The good maintenance of rectangular shape suggests the good supercapacitor performance at high charging-discharging rate. The reason for the outstanding performance of EEG are from the large lateral size and high electrical conductivity.

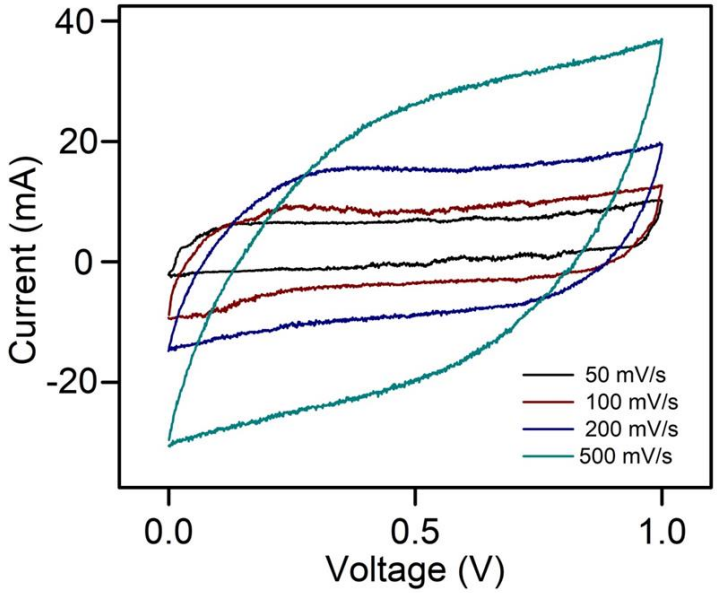

Figure 26: CV curves of graphene-based supercapacitors at various scan rates

To fully evaluate the cost of stored energy from supercapacitors based on EEG and other graphene sources. **Table 2** summarized the supercapacitor performance based on EEG and other commercial graphene and the cost to store energy for each graphene sources. It is obvious that reduced graphene oxide has the highest energy density, which comes from the very high surface area of rGO. However, the high price of rGO will deter the commercial usage for supercapacitor application. Among all the other graphene nanoplatelets sources and EEG, EEG has the lowest cost to store energy. The reasons are the low cost of EEG production approach and big lateral size of final EEG products.

Table 2: Comparison of supercapacitor performance based on various graphene sources

Graphene sources	**Sigma-Aldrich**	**Knano**	**Graphene Supermarket**	**ACS Material**	**TAMU**
Graphene type	reduced graphene oxide	graphene nanoplatelets			**EEG**
Price ($/g)	464	3	4	1.6	**6**
Specific capacitance (F/g)	100-150	13	8	15	**57**
Energy density (Wh/kg)	14-21	1.8	1.1	2.1	**7.9**
Stored energy cost ($/Wh)	22K-33K	1.7K	3.6K	0.8K	**0.7K**

CHAPTER V

CONCLUSION AND FUTURE WORK

5.1 Conclusion

In order to bring graphene to the world and apply this technology into our daily lives, great strides must be made in the scalability, functionalization, and tunability of graphene. As mentioned previously, the scalability of high-quality graphene production has been the primary focus of graphene research. Being able to produce graphene with a large lateral size and few defects will facilitate development of graphene applications and commercialization of these products.

The purpose of our research is to show the scalability of the second-generation reactor design, as well as apply the produced material to supercapacitor technology. From the results of our experiments, we can conclude that:

(1) The initial graphite bed thickness can limit the ability of electrolyte solution to diffuse through the reactor. Additionally, if the graphite bed thickness is decreased, the graphite bed will no longer act as a conductive monolith. However, the reactor volume can be increased by extending the reactor in the lateral directions.

(2) The reaction rate is important to the design and scalability of the electrochemical reactor. While the reaction continues to progress linearly until 240 minutes, the reaction proceeds the fastest in the initial 30 minutes.

5.2 Future Work

In prior studies of graphite-to-graphene exfoliation using mechanical exfoliation, the crystallinity of the parent graphite structure has a considerable effect on both the processability and morphology of the as-produced graphene.[102, 103] No data currently exist for any electrochemical exfoliation method capable of processing powders because it has never been done before. With the method described above, we propose to study how the parent graphite powder crystallinity and morphology affects the final product. We hypothesize that the initial grain size will be correlated with the lateral size of the as-produced graphene because the method itself does not tend to break the graphene nanosheets and decrease the lateral area (whereas mechanical shear or sonication is known to do so). Graphite wettability will be discussed in further detail below. We will investigate the following source graphite types: highly oriented pyrolytic graphite (HOPG), flake graphite, expandable flake graphite (pre-intercalated with sulfates), synthetic graphite, and natural (amorphous) graphite.

A semi-batch roll-to-roll reactor concept is proposed based on the studies on the second-generation reactor (**Figure 27**). Graphite flakes will be packed into the dialysis bag with graphite foil (acting as the working electrode). Shown in **Figure 28**, the membrane will be rolled into the electrolyte bath and sealed at two ends in order to prevent graphite leakage. Then the counter electrodes will be compressed around the reaction section to create a compacted, conductive monolith. A positive voltage will be applied through the graphite foil to being the reaction process. After the residence time, the voltage will be cut off and the external pressure will be released. The dialysis bag can

be rolled through the reaction area and the process can be repeated. The exfoliated graphite can be transferred to a washing and separation unit operation. The unexfoliated graphite and disintegrated graphite foil can be recycled into the graphite feed stock and exfoliated again.

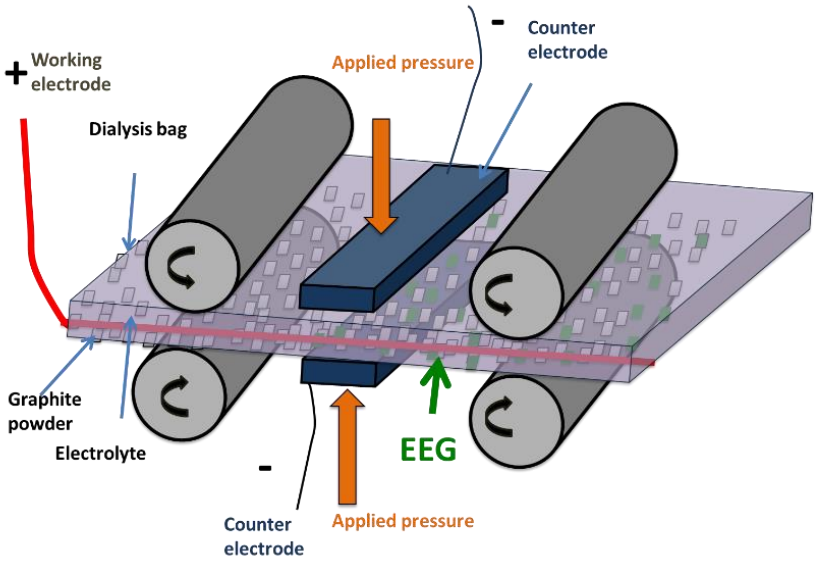

Figure 27: Schematic of a semi-batch roll-to-roll concept for the production of graphene from graphite flakes through the electrochemical containment exfoliation method

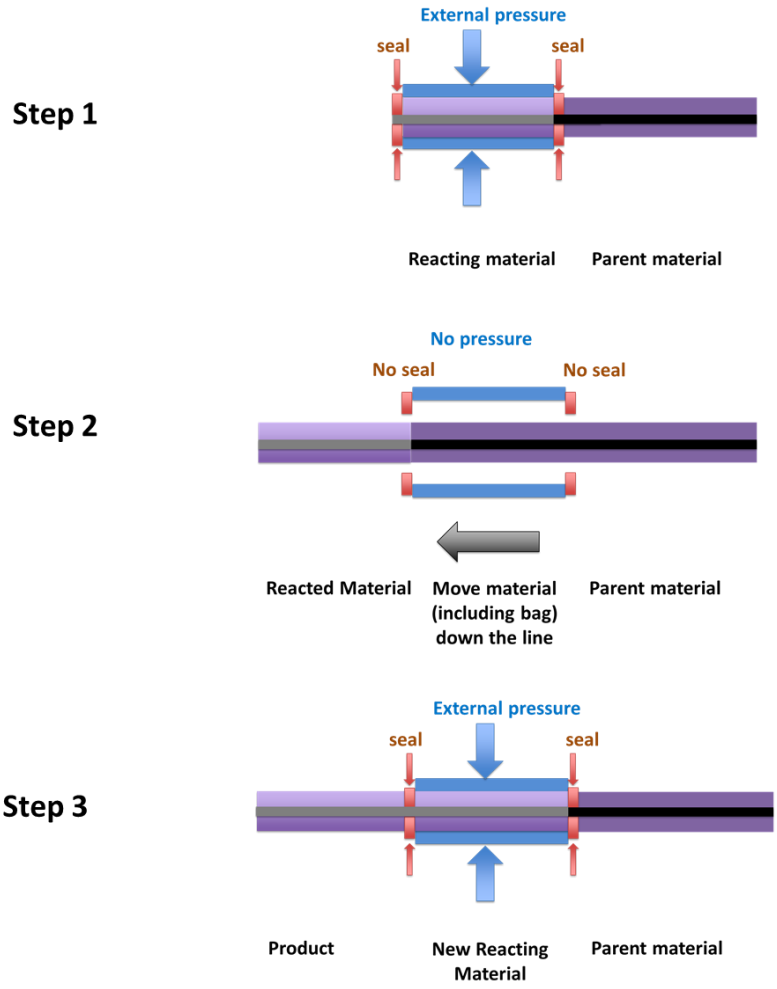

Figure 28: Schematic depicting the process for a semi-batch roll-to-roll packed bed reactor

REFERENCES

1. Day, C. *Andre Geim and Konstantin Novoselov win 2010 physiscs Nobel for graphene*. 2010. DOI: 10.1063.

2. Geim, A.K., Novoselov, K. S., *The rise of graphene.* Nature Materials, 2007. **6**.

3. Parvez, K., *et al*., *Exfoliation of Graphite into Graphene in Aqueous Solutions of Inorganic Salts.* Journal of the American Chemical Society, 2014. **136**(16): p. 6083-6091.

4. Allen, M.J., V.C. Tung, and R.B. Kaner, *Honeycomb carbon: a review of graphene.* Chemical reviews, 2009. **110**(1): p. 132-145.

5. Losurdo, M., *et al*., *Graphene CVD growth on copper and nickel: role of hydrogen in kinetics and structure.* Physical Chemistry Chemical Physics, 2011. **13**(46): p. 20836-20843.

6. Bin Wu, D.G., Zhiping Xu, Yunlong Guo, Liping Huang, Yunzhou Xue, Jianyi Chen, Gui Yu, Yunqu Liu, *Self-organized graphene crystal patterns.* NPG Asia Materials, 2013. **5**(36): p. 7.

7. Ghaffarzadeh, K., *Graphene, 2D Materials and Carbon Nanotubes: Markets, Technologies and Opportunities 2016-2026.* http://www.idtechex.com/research/reports/graphene-2d-materials-and-carbon-nanotubes-markets-technologies-and-opportunities-2016-2026-000465.asp, (retrieved Dec 27 2016).

8. Pumera, M., *Graphene-based nanomaterials for energy storage.* Energy & Environmental Science, 2011. **4**(3): p. 668-674.

9. Huang, X., *et al*., *Graphene-based composites.* Chemical Society Reviews, 2012. **41**(2): p. 666-686.

10. Boukhvalov, D.W., M.I. Katsnelson, and A.I. Lichtenstein, *Hydrogen on graphene: Electronic structure, total energy, structural distortions and magnetism from first-principles calculations.* Physical Review B, 2008. **77**(3): p. 035427.

11. Novoselov, K.S., *et al*., *Electric field effect in atomically thin carbon films.* Science, 2004. **306**(5696): p. 666-669.

12. Chen, L.F., *et al*., *Thermal properties of epoxy resin based thermal interfacial materials by filling Ag nanoparticle-decorated graphene nanosheets.* Composites Science and Technology, 2016. **125**: p. 17-21.

13. Wu, S.L., T.J. Shi, and L.Y. Zhang, *Latex co-coagulation approach to fabrication of polyurethane/graphene nanocomposites with improved electrical conductivity, thermal*

conductivity, and barrier property. Journal of Applied Polymer Science, 2016. **133**(11): p. 13.

14. Jason Stafford, A.P., Nwachukwu Uzo, Omar K. Matar, and Camille Petit, *Towards Scale-up of Graphene Production via Nonoxidizing Liquid Exfoliation Methods.* AIChE Journal, 2018. **64**(9): p. 31.

15. Parviz, D., *et al*., *Challenges in Liquid-Phase Exfoliation, Processing, and Assembly of Pristine Graphene.* Advanced Materials, 2016. **28**(40): p. 8796-8818.

16. Thomas Achee, W.S., Joshua Hope, Samuel Quitzau, Charles Brandon Sweeney, Smit Shah, Touseef Habib, Micah Green, *High-yield scalable graphene nanosheet production from compressed graphite using electrochemical exfoliation.* Scientific Reports, 2018. **8**(14525): p. 8.

17. Connon, S. *The graphene story: how Andrei Geim and Kostya Novoselov hit on a scientific breakthrough that changed the world... by playing with sticky tape*. 2013.

18. Rincon, P. *How sticky tape trick led to Nobel Prize*. 2010.

19. Jannik C. Meyer, A.K.G., M. I. Katsnelson, K. S. Novoselov, T. J. Booth, S. Roth, *The structure of suspended graphene sheets.* Nature, 2007. **446**: p. 4.

20. Landau, L., *Zur Theorie der phasenumwandlungen II.* Phys. Z. Sowjetunion, 1937. **11**(545): p. 36-35.

21. Peierls, R., *Quelques propriétés typiques des corps solides.* Annales de l'I. H. P.,, 1935. **5**(3): p. 177-222.

22. Alan P. Kauling, A.T.S., Diego P. Pisoni, Roshini C. Pradeep, Ricardo Bentini, Ricardo V. B. Oliveira, Konstantin S. Novoselov, Antonio H. Castro Neto, *The Worldwide Graphene Flake Production.* Advanced Matrerials, 2018: p. 6.

23. *The Nobel Prize in Physics 2010*. 2010, The Nobel Prize: NobelPrize.org.

24. Z. Sun, S.K.H., M. Boneshanscher, J. Sainio, J. Lahtinen, P. Liljeroth, D. Vanmaekelbergh, *The atomic and electronic structure of graphene and graphene nanocrystals*.

25. Zan, R., *Microscopy and Spectroscopy of Graphene: Atomic Scale Structure and Interaction with Foreign Atom Species*, in *School of Physics and Astronomy*. 2012, University of Manchester. p. 170.

26. Fasolino, A., J.H. Los, and M.I. Katselson, *Intrinsic Ripples in graphene.* Nature Materials, 2007. **6**: p. 4.

27. A.H. Castro Neto, F.G., N.M.R. Peres, K.S. Novoselov, and A. K. Geim, *The Electronic Properties of Graphene.* Reviews of Modern Physics, 2009. **81**.

28. Standardization, I.O.f., *Nanotechnologies - Vocabulary*, in *Part 13: Graphene and related two-dimensional (2D) materials*. 2017, International Organizaiton for Standardization. p. 21.

29. Jingang Wang, F.M., Wenie Liang, Mentao Sun, *Electrical Properties and applications of graphene, hexagonal boron nitride (h-BN), and graphene/h-BN heterostructures.* Materials Today Physics, 2017. **2**(September): p. 29.

30. Dreyer, D.R., *et al*., *The chemistry of graphene oxide.* Chemical Society Reviews, 2010. **39**(1): p. 228-240.

31. Florian Banhart, J.K., Arkady V. Krasheninnikov, *Structural Defects in Graphene.* ACS Nano, 2010. **5**(1): p. 16.

32. Dimitrios G. Papageorgiou, I.A.K., Robert J. Young, *Mechanical properties of graphene and graphene-based nanocomposites*, in *Progress in Materials Science*. 2017, ELSEVIER: ScienceDirect. p. 53.

33. Eric Pop, V.V., Ajit K. Roy, *Thermal Properties of Graphene: Fundamentals and Applications.* MRS Bulletin, 2012. **37**: p. 1273-1281.

34. Lindsay, L., D.A. Broido, and N. Mingo, *Flexural Phonons and Thermal transport in graphene.* Physical Review B, 2010. **115427**: p. 6.

35. Lindsay, L., D.A. Broido, and N. Mingo, *Diameter dependence of carbon nanotube thermal conductivity and extension to the graphene limit.* Physical Review B, 2010. **161402**.

36. Virendra Singh, D.J., Lei Zhai, Soumen, Das, Saiful I. Khondaker, Sudipta Seal, *Graphene based materials: Past, present, and future.* Progress in Materials Science, 2011. **56**: p. 94.

37. Jin-Feng Dai, G.-J.W., Lang Ma, Cheng-Ken Wu, *Surface Properties of Graphene: Relationship to Graphene-Polymer Composites.* Review Advanced Materials Science, 2015. **40**: p. 60-71.

38. Alain Peigney, C.L., Emmanuel Flahaut, Revathi Bacsa, Abel Rousset, *Specific surface area of carbon nanotubes and bundles of carbon nanotubes.* Carbon, 2001. **39**: p. 8.

39. Mei-xian Wang, Q.L., Hong-fan Sun, Eric A. Stach, Jian Xie, *Preparation of High Surface Area Nano-Structured Graphene Composites.* ECS Transactions, 2012. **41**(22): p. 11.

40. Maocong Hu, Z.Y., and Xianqin Wang, *Characterization techniques for graphene-based materials in catalysis.* AIMS Materials Science, 2017: p. 34.

41. *Single Layer Graphene*. 2018 [cited 2019; Available from: https://www.acsmaterial.com/single-layer-graphene-graphene-factory-1045.html.

42. Wall, M., *The Raman Spectroscopy of Graphene and the Determination of Layer Thickness*, T. Scientific, Editor. 2011, Semantic Scholar.

43. Ferrari, A.C., *et al*., *Raman spectrum of graphene and graphene layers.* Physical review letters, 2006. **97**(18): p. 187401.

44. Jianfeng Shen, B.Y., Min Shi, Hongwei Ma, Na Li, Mingxin Ye, *One step hydrothermal synthesis of TiO_2-reduced graphene oxide sheets.* Journal of Materials Chemistry, 2011. **21**: p. 7.

45. Rebeccas S. Edwards, K.S.C., *Graphene Synthesis: relationship to applications.* Nanoscale, 2013(1): p. 14.

46. Commission, E., *Graphene and Human Brain Project win largest research excellence award in history, as battle for sustained science funding continues*. 2013, European Commission.

47. Karim, N. *Graphene phase modulators hold the key to faster mobile technology*. 2018; Available from: https://graphene-flagship.eu/garphene-phase-modulators-hold-the-key-to-faster-mobile-technology.

48. Khaled Parvez, R.L., Sreenicasa Reddy Puniredd, Yenny Hernandez, Felix Hinkel, Suhao Wang, Xinliang Feng, Klaus Mullen, *Electrochemically Exfoliated Graphene as Solution-Processable, Highly Conductive Electrodes for Organic Electronics.* ACS Nano, 2013. **7**(4): p. 3598-3606.

49. Schwierz, F., *Graphene Transistors.* Nature Nanotechnology, 2010: p. 487-496.

50. Lloyd, S. *Graphene Interface Engineering for Large Area, High Efficiency Solar Cells*. 2018; Available from: https://graphene-flagship.eu/large-area-pscs.

51. *Perovskite Solar*. 2018 [cited 2019; Available from: https://www.perovskite-info.com/perovskite-solar.

52. Miller, J.R. and P. Simon, *Electrochemical Capacitors for Energy Management.* Science, 2008. **321**: p. 651-653.

53. Simon, P. and Y. Gogotsi, *Materials for electrochemical capacitors.* Nature, 2008. **7**: p. 845-854.

54. Liu, C., *et al*., *Advanced Materials for Energy Storage.* Advanced Energy Materials, 2010. **22**(8): p. 28-62.

55. Kaempgen, M., *et al*., *Printable Thin Film Supercapacitors Using Singe-Walled Carbon Nanotubes.* Nano Letters, 2009. **9**(5): p. 1872-1876.

56. Winter, M. and R.J. Brodd, *What are Batteries, Fuel Cells, and Supercapacitors?* Journal of Chemical Reviews, 2004. **104**: p. 4245-4269.

57. Don N. Futaba, K.H., Takeo Yamada, Tatsuki Hiraoka, Yuhei Hayamizu, Yozo Kakudate, Osamu Tanaike, Hiroaki Hatori, Motoo Yumura & Sumio Iijima, *Shape-engineerable and highly densely packed single-walled carbon nanotubes and their applicaiton as super-capacitor electrodes.* Nature Materials, 2006. **5**: p. 987-994.

58. Zhang, L.L., R. Zhou, and X.S. Zhao, *Graphene-based materials as supercapacitor electrodes.* Royal Society of Chemistry, 2010. **20**: p. 5983-5992.

59. Liu, C., *et al*., *Graphene-based supercapacitor with an Ultrahigh energy density.* Nano Letters, 2010. **10**(12): p. 4863-4868.

60. Shi, W., *et al*., *Achieving high specific charge capacitances in Fe3O4/reduced graphene oxide nanocomposites.* Journal of Materials Chemistry, 2011. **21**: p. 3422-3427.

61. Hu, C.-C., *et al*., *Design and Tailoring of the Nanotubular Arrayed Architecture of Hydrous RuO2 for Next Generation Supercapacitors.* Nano Letters, 2006. **6**(12): p. 2690-2695.

62. Kumar, B.V.N., *et al*. *Synthesis and characterization of copeer particles decorated reduced graphene oxide nano composites for the application of supercapacitors*. in *AIP*. 2018.

63. Xiao, W., J.Y.H. Fuh, and L. Lu, *Growth of single-crystal α-MnO2 nanotubes prepared by a hydrothermal route and their electrochemical properties.* Journal of Power Sources, 2009. **193**(2): p. 935-938.

64. Arbizzani, C., M. Mastragostino, and L. Meneghello, *Polyer-based redox supercapacitors: A comparative study.* Electrochimica Acta, 1996. **41**(1): p. 21-26.

65. Ryu, K.S., *et al*., *Symmetric redox supercapacitors with conducting polyaniline electrodes.* Journal of Power Sources, 2002. **103**(2): p. 305-309.

66. Wu, X., *et al*., *Template synthesis of hollow fusiform RuO2*xH2O nanostructure and its supercapacitor performance.* Royal Society of Chemistry, 2012: p. 469-472.

67. Mendoza-Sanchez, B., *et al*., *An investigation of nanostructured thin film α-MoO3 based supercapacitor electrodes in an aqueous electrolyte.* Electrochimica Acta, 2012. **91**: p. 253-260.

68. Brousse, T., *et al*., *Crystalline MnO2 as Possible Alternatives to Amorphous compounds in Electrochemical Supercapacitors.* Journal of The Electrochemical Society, 2006. **153**(12): p. 2171-2180.

69. Fumiya Mori, M.K., and Yoshihiko Arao, *Effect of graphite structures on the productivity and quality of few-layer graphene in liquid-phase exfoliation.* J Material Science, 2018(53): p. 9.

70. Paredes, J.I., *et al*., *Graphene Oxide Dispersions in Organic Solvents.* Langmuir, 2008. **24**(19): p. 10560-10564.

71. Marcano, D.C., *et al*., *Improved synthesis of graphene oxide.* ACS nano, 2010. **4**(8): p. 4806-4814.

72. Heyong He, J.K., Michael Foster, Anton Lerf, *A new structural model for graphite oxide.* Chemical Physics Letters, 1998. **287**(1-2): p. 53-56.

73. Szabó, T., *et al*., *Evolution of Surface Functional Groups in a Series of Progressively Oxidized Graphite Oxides.* Chemistry of Materials, 2006. **18**(11): p. 2740-2749.

74. Erickson, K., *et al*., *Determination of the Local Chemical structure of Graphene Oxide and Reduced Graphene Oxide.* Advanced Materials, 2010. **22**: p. 4467-4472.

75. Gao, W., *et al*., *New insights into the structure and reduction of graphite oxide.* Nature Chemistry, 2009. **1**.

76. William S. Hummers Jr., R.E.O., *Preparation of Graphitic Oxide.* Journal of the Amercian Chemistry Society, 1958. **80**(6): p. 1.

77. Sasha Stankovich, D.A.D., Richard D. Piner, Kevin A. Kohlhaas, Aldred Kleinhammes, Yuanyuan Jia, Yue Wu, SonBinh T. Nguyen, Rodney S. Ruoff, *Synthesis of graphene-based nanosheets via chemical reduction of exfoliated graphite oxide.* Carbon, 2007. **45**: p. 8.

78. Meiping, Y., *3 students injured after blast in lab*, in *Shanghai Daily*. 2016.

79. Buchsteiner, A., A. Lerf, and J. Pieper, *Water Dynamics in Graphite Oxide Investigated with Neutron Scattering.* The Journal of Physical Chemistry, 2006. **110**(45): p. 22328-22338.

80. Gomez-Navarro, C., M. Burghard, and K. Kern, *Elastic Properties of Chemically Derived Single Graphene Sheets.* Nano Letters, 2008. **8**(7): p. 2045-2049.

81. Jasim, D.A., *et al*., *Thickness of funcitonalized graphene oxide sheets plays critical role in tissue accumulation and urinary excretion: A pilot PET/CT study.* Applied Materials Today, 2016. **4**: p. 24-30.

82. Rourke, J.P., *et al*., *The Real Graphene Oxide Revealed: Stripping the Oxidative Debris from the Graphene-like Sheets.* Angewandte Chemie, 2011. **50**(14): p. 3173-3177.

83. Eda, G., G. Fanchini, and M. Chhowalla, *Large-area ultrathin films of reduced graphene oxide as a transparent and flexible electronic material.* Nature Nanotechnology, 2008. **3**: p. 270-274.

84. Eda, G. and M. Chhowalla, *Chemically Derived Graphene Oxide: Towards Large-Area Thin-Film Electronics and Optoelectronics.* Advanced Materials, 2010. **22**(22): p. 2392-2415.

85. .Becerril, H.A., *et al*., *Evaluation of Solution-Processed Reduced Graphene Oxide Films as Transparent Conductors.* ACS Nano, 2008. **2**(3): p. 46-470.

86. Robinson, J.T., *et al*., *Wafer-scale Reduced Graphene Oxide FIlms for Nanomechanical Devices.* Nano Letters, 2008. **8**(10): p. 3441-3445.

87. Paton, K.R., *et al*., *Scalable production of large quantities of defect-free few-layer graphene by shear exfoliation in liquids.* Nature Materials, 2014. **13**(6): p. 624-630.

88. Dhanraj B. Shinde, J.B., Christopher D. Easton, Rico F. Tabor, Adrian Neild, and Mainak Majumder, *Shear Assisted Electrochemical Exfoliation of Graphite to Graphene.* Langmuir, 2016(32): p. 8.

89. Kyler S Rountree, S.A.S., Charles B Sweeney, Fahmida Irin, and Micah J Green, *Graphene Reflux: Improving the yield of liquid-exfoliated nanosheets through repeated separation techniques.* Nanotechnology, 2016(27): p. 6.

90. Tran, T.S., *et al*., *High shear-induced exfoliation of graphite into high quality graphene by Taylor-Couette flow.* RSC Advances, 2016(15): p. 12003-12008.

91. Israelachvili, J.N., *Intermolecular and Surface Forces*. Revised 3rd Edition ed. 2011: Academic Press.

92. Du, W., *et al*., *Organic salt-assisted liquid-phase exfoliation of graphite to produce high-quality graphene.* Chemical Physics Letters, 2013. **568-569**: p. 198-201.

93. Youning Gong, Y.P., Delong Li, Chengzhi Luo, Xuefeng Ruan, Qiang Fu, Chunxu Pan, *Preparation of high-quality graphene via electrochemcial exfoliation & spark plasma sintering and its applications.* Applied Surface Science, 2016(397): p. 7.

94. Mario Hoffman, W.-Y.C., Tuan D Nguyn, and Ya-Ping Hsieh, *Controlling the properties of graphene produced by electrochemical exfoliation.* Nanotechnology, 2015(26): p. 6.

95. Liu, J., *et al*., *Improved synthesis of graphene flakes from the multiple electrochemical exfoliation of graphite rod.* Nano Energy, 2013. **2**(3): p. 377-386.

96. Abdelkader, A.M., I.A. Kinloch, and R.A.W. Dryfe, *Continuous Electrochemical Exfoliation of Micrometer-Sized Graphene Using Synergistic Ion Intercalations and Organic Solvents.* ACS Applied Materials & Interfaces, 2014. **6**(3): p. 1632-1639.

97. Wu, H., *et al*., *One-step in situ ball milling synthesis of polymer-functionalized graphene nanocomposites.* Journal of Materials Chemistry, 2011. **21**(24): p. 8626-8632.

98. Zhang, S., Y. Li, and N. Pan, *Graphene based supercapacitor fabricated by vacuum filtration deposition.* Journal of Power sources, 2012. **206**: p. 476-482.

99. Lee, J.H., *et al*., *Restacking-inhibited 3D reduced graphene oxide for high performance supercapacitor electrodes.* ACS nano, 2013. **7**(10): p. 9366-9374.

100. Achee, T.C., *et al*., *Electrochemically expanded materials and reactor for producing the same*. August 8, 2016.

101. Buglione, L., *et al*., *Graphene materials preparation methods have dramatic influence upon their capacitance.* Electrochemistry Communications, 2012. **14**(1): p. 5-8.

102. Botas, C., *et al*., *Optimization of the size and yield of graphene oxide sheets in the exfoliation step.* Carbon, 2013. **63**: p. 576-578.

103. Yi, M. and Z. Shen, *A review on mechanical exfoliation for the scalable production of graphene.* Journal of Materials Chemistry A, 2015. **3**(22): p. 11700-11715.